JOURNAL OF GEOPHYSICAL RESEARCH, VOL. 112, D18205, doi:10.1029/2006JD008175, 2007

Satellite-derived aerosol optical depth over dark water from MISR and MODIS: Comparisons with AERONET and implications for climatological studies

Ralph A. Kahn,[1] Michael J. Garay,[1] David L. Nelson,[1] Kevin K. Yau,[1] Michael A. Bull,[1] Barbara J. Gaitley,[1] John V. Martonchik,[1] and Robert C. Levy[2]

Received 23 October 2006; revised 30 March 2007; accepted 26 June 2007; published 26 September 2007.

[1] Although the current Multiangle Imaging Spectroradiometer (MISR) and Moderate Resolution Imaging Spectroradiometer (MODIS) satellite passive remote sensing midvisible aerosol optical thickness (AOT) products are accurate overall to about 0.05 or 20%, they differ systematically on a global, monthly average basis, by about 0.03 to 0.05. Some key climate change and other applications require accuracies of 0.03 or better. The instruments are sufficiently stable and well characterized, and have adequate signal-to-noise, to realize such precision. However, assumptions made in the current standard aerosol retrieval algorithms produce AOT biases that must be addressed first. We identify the causes of AOT discrepancies over dark water under typical, relatively low AOT conditions and quantify their magnitudes on the basis of detailed analysis. Examples were selected to highlight key issues for which there are coincident MISR, MODIS, and Aerosol Robotic Network (AERONET) observations. Instrument calibration and sampling differences, assumptions made in the MISR and MODIS standard algorithms about ocean surface boundary conditions, missing particle property or mixture options, and the way reflectances used in the retrievals are selected each contribute significantly to the observed differences under some circumstances. Cloud screening is also identified as a factor, though not fully examined here, as are the relatively rare high-AOT cases over ocean. Specific algorithm upgrades and further studies indicated by these findings are discussed, along with recommendations for effectively using the currently available products for regional and global applications.

Citation: Kahn, R. A., M. J. Garay, D. L. Nelson, K. K. Yau, M. A. Bull, B. J. Gaitley, J. V. Martonchik, and R. C. Levy (2007), Satellite-derived aerosol optical depth over dark water from MISR and MODIS: Comparisons with AERONET and implications for climatological studies, *J. Geophys. Res.*, *112*, D18205, doi:10.1029/2006JD008175.

1. Introduction

[2] The Multiangle Imaging Spectroradiometer (MISR) [*Diner et al.*, 1998] began taking data in late February 2000. Since then, numerous studies have compared aerosol optical thickness (AOT) retrieved from the instrument's 36 spectral angular channels with similar quantities derived from the Aerosol Robotic Network (AERONET) [*Holben et al.*, 1998] Sun photometer network, the Moderate Resolution Imaging Spectroradiometer (MODIS) [*Barnes et al.*, 1998; *Salomonson et al.*, 1989] that flies aboard the Terra satellite with MISR, and other regional and global observations [e.g., *Abdou et al.*, 2005; *Christopher and Wang*, 2004; *Diner et al.*, 2001; *Kahn et al.*, 2005a, 2005b; *Liu et al.*, 2004; *Martonchik et al.*, 2004; *Myhre et al.*, 2005; *Redemann et al.*, 2005; *Schmid et al.*, 2003; *Yu et al.*, 2006]. That work demonstrates the MISR Standard Aerosol Retrieval algorithm (V16 or lower) retrieves AOT over land and water, with overall statistical accuracy better than 0.05 or 20%, whichever is larger, and with greater accuracy over some surfaces such as dark water. Similar results are reported for MODIS-AERONET AOT comparisons [*Remer et al.*, 2005; *Levy et al.*, 2003, 2005; *Chu et al.*, 2002; L. A. Remer et al., 2006, Algorithm for remote sensing of tropospheric aerosol from MODIS: Collection 5, available at http://modis-atmos.gsfc.nasa.gov/reference_atbd.php; hereinafter referred to as Remer et al., 2006].

[3] However, some blunders occur, often because of inadequate cloud screening or inaccurate surface property assumptions, and persistent small but systematic differences between MISR and MODIS AOT values can be significant when large aggregates of measurements from the two instruments are compared. MODIS produces generally higher midvisible AOT than MISR and AERONET over land, whereas MISR AOT is generally higher than MODIS over water [e.g., *Abdou et al.*, 2005; *Myhre et al.*, 2005]. Recent improvements in MISR band-to-band and camera-to-camera calibration have reduced average MISR-

[1]Jet Propulsion Laboratory, California Institute of Technology, Pasadena, California, USA.
[2]NASA Goddard Space Flight Center, Greenbelt, Maryland, USA.

0148-0227/07/2006JD008175$09.00

AERONET low-light-level retrieved AOT discrepancies from about 0.05 to 0.025 [*Bruegge et al.*, 2003; *Diner et al.*, 2004b; *Kahn et al.*, 2005b]. The resulting midvisible AOT values can be used for many applications. However, the remaining MISR-MODIS monthly global average AOT differences, of order 0.02 to 0.05 in the long-term record [e.g., *Mishchenko et al.*, 2007], limit the confidence with which the data can be applied to large-spatial-scale and long-term climate issues, where accuracies of 0.01 to 0.03 are required, for example, to achieve about 0.5 Wm^{-2} aerosol climate forcing sensitivity [e.g., *Kahn et al.*, 2005b].

[4] Among the likely contributors to the systematic residual MISR-MODIS AOT discrepancies are differences in absolute radiometric calibration, cloud screening, algorithm assumptions about aerosol microphysical properties and surface boundary conditions, as well as sampling. To better understand the underlying causes of the AOT discrepancies, and to point toward possible algorithm upgrades, we study in detail five cases where MISR and MODIS both acquired data over dark water, near coincident with AERONET island stations. The cases were selected to capture the key differences we observe, allowing us to test the underlying algorithm assumptions. Agreement between these data sets is generally higher than in these cases, as discussed in the references above.

[5] We use a forward radiative transfer model [*Martonchik et al.*, 1998] and the MISR Research Aerosol Retrieval algorithm [*Kahn et al.*, 2001a] to test hypotheses about aerosol property and surface boundary condition assumptions. Absolute calibration, including a known ~3% difference in the radiance scales adopted by MISR and MODIS at midvisible wavelengths, larger in the blue and decreasing to ~0.8% in the MISR near-infrared band, is discussed as needed, but is treated more fully elsewhere [e.g., *Lyapustin et al.*, 2007; *Bruegge et al.*, 2003]. Since MISR, MODIS, and AERONET must all report cloud-free aerosol retrievals to be used in the present study, satellite aerosol retrieval cloud-masking approaches are not comprehensively sampled by cases that meet the coincidence requirements applied here; this issue is addressed more fully in a separate study.

[6] In this paper, we go into a fair amount of detail about the MISR and MODIS aerosol retrieval algorithms, as is required to understand subtle differences in the results that matter when these data are used to assess climate trends. Although a comprehensive statistical study is beyond the scope of the paper, it is part of continuing work. A study of this type, looking at MODIS and Sun photometer data [*Zhang and Reid*, 2006], reached conclusions similar to ours regarding wind speed assumptions, and provides statistical assessments of aerosol type assumptions and cloud contamination effects for MODIS. We also focus on the recently released MODIS Collection 5 data products (Remer et al., 2006), but include Collection 4 results for comparison, since the previously published statistical and physical analyses of MODIS aerosol products, referenced above, used Collection 4 data. Throughout this paper, Collection 5 (C5) MODIS data are used, unless explicitly labeled Collection 4 (C4).

[7] The current paper is aimed at assessing the possible significance of likely causes for MISR and MODIS AOT discrepancies, using a direct physical approach, for situations where retrievals from both instruments and ground truth are available. Section 2 briefly reviews the MISR, MODIS, and AERONET data sets and algorithm assumptions, emphasizing those that play major roles in the investigations that follow. Section 3 presents five case-by-case analyses aimed at identifying and explaining the observed differences to the extent possible. Section 4 contains a synthesis of the results, suggestions about how the current satellite aerosol products might be used for large-scale and long-term studies, and a summary of what we might expect from refined products.

2. MISR, MODIS, and AERONET Data

[8] Table 1 lists the events selected for analysis. They all occur at deep ocean sites near islands hosting AERONET Sun and sky-scanning photometers: Ascension Island, Forth Crete, and Tahiti. The cases exhibit relatively cloud-free conditions, when MISR, MODIS, and AERONET all acquired good data, and when the MODIS view was glint-free within at least part of the 400 km wide MISR swath near the AERONET site. The cases also capture the discrepancy patterns we find among MISR, MODIS, and AERONET AOT over water in the larger data sets. Table 1 also lists key environmental conditions, obtained from other sources, and used as constraints in the analyses here.

2.1. MISR and MODIS

[9] MISR radiances were extracted from the V24 Level 1B2 data product, and aerosol retrievals were obtained from the V17 Standard Aerosol Retrieval product, both available through the NASA Langley Atmospheric Sciences Data Center (http://eosweb.larc.nasa.gov/). MODIS radiances were extracted from the Collection 5 MOD02 1KM products, whereas the geolocation (MOD03) and Standard Aerosol Retrieval (MOD04) results were obtained for both the Collection 4 and 5 products, available from the NASA Goddard Space Flight Center Earth Sciences Data and Information Services Center (GES DISC, http://daac.gsfc.nasa.gov/ for Collection 4), and the Level 1 and Atmosphere Archive and Distribution System (LAADS, http://ladsweb.nascom.nasa.gov/ for Collection 5). For both MISR and MODIS the patch average radiance values were converted to equivalent reflectances according to

$$\rho_{MI,MO}(\lambda,\mu) = L_{MI,MO}(\lambda,\mu) \times \pi D^2 / E_{0MI,MO}(\lambda) \quad . \qquad (1)$$

Here MI, MO represents MISR or MODIS, as appropriate, λ indexes the instrument spectral band, and μ references the cosine of the satellite view angle. $L_{MI,MO}$ is the measured radiance value, D is the Earth-Sun distance in AU at observation time, and $E_{0MI,MO}$ is the band-weighted solar irradiance at top of atmosphere (TOA) for average Earth-Sun separation ($D = 1$). Note that the equivalent reflectances given by equation (1), when normalized via dividing by the cosine of the solar zenith angle, become bidirectional reflectance factors (BRFs). Also the data number–to-equivalent-reflectance conversion factors given in the MODIS product contain the required D and E_0 adjustments. Tables 2a and 2b list the MISR, MODIS, and AERONET bands used, their effective wavelengths, and E_0 values for the MISR and MODIS channels. The E_0 values adopted by

Table 1. Ocean Cases Having Coincident MISR, MODIS, and AERONET Data Used in This Study

Island Site	Date	Time, UTC	Latitude	Longitude	Sun Zenith Angle	Cameras in Sun Glint[a]	Terra Orbit	MISR Path/Block	MODIS Granule	AERONET AOT, 558 nm	Wind[b], m/s, Ave/Max	P_0[b], mb	T_0[b], C, Ave	H_2O_v[c], cm	Ozone[c], DU	Airmass Type[d]	AOT Pattern[e]
Forth Crete	13 Sep 2003	0904	35.33°N	25.28°E	35.4	Bf, Af	19878	180/62	A2003256.0900	0.11	3.6/7.5	1011	27	2.6	287	continental	MO ≈ MI > AR
Ascension	18 Feb 2005	1119	07.98°S	14.42°W	28.3	(An)	27510	200/97	A2005049.1115	0.21	5.8/9.2	1013	29	3.3	258	mostly maritime	AR > MI ≈ MO
Ascension	1 Jan 2005	1117	07.98°S	14.42°W	29.3	none	26811	200/97	A2005001.1115	0.12	4.7/8.9	1015	27	3.0	260	mostly maritime	AR ≈ MI > MO
Tahiti	12 Aug 2001	2022	17.58°S	149.95°W	40.7	Aa, Ba, Ca, Da	8788	053/104	A2001224.2020	0.06	1.1/5.0	1016	28	3.6	273	maritime	MI ≥ MO ≫ AR
Tahiti	3 Sep 2003	2013	17.58°S	149.95°W	35.9	Aa, Ba, Ca	19739	053/104	A2003246.2010	0.05	1.4/3.6	1016	28	3.8	259	maritime	MI >∼ AR > MO

[a]An = nadir; Af, Aa = 26.1° fore and aft; Bf, Ba = 45.6° fore and aft; Cf, Ca = 60.0° fore and aft; Df, Da = 70.5° fore and aft. Sun glint contamination was assessed using a 40° view angle threshold around the specular direction; in addition, the patch radiance variance must be <1% for that view. For the Ascension 18 February 2005 case the nadir camera is 39° from the glint vector, but the variance criterion indicates no glint contamination.

[b]Near-surface wind, pressure, and temperature obtained from the Weather Underground online archive (http://www.wunderground.com/). Note that there is uncertainty in the wind speed that should be used to describe sea-surface state. Measurements near coasts and from space-based scatterometer measurements can differ by several m/s, and wind speed changes take time to manifest on the surface. The numbers given here are reported daily average and maximum.

[c]Water vapor column abundance obtained from Aerosol Robotic Network (AERONET) retrievals; ozone column abundance obtained from the Earth Probe Total Ozone Mapping Spectrometer (TOMS) data archive (http://toms.gsfc.nasa.gov/ozone/ozone.html).

[d]Hybrid Single-Particle Lagrangian Integrated Trajectory (HYSPLIT) model (Draxler and Rolph, 2003), obtained from the READY website (http://www.arl.noaa.gov/ready.html). "Mostly maritime" means that air at some level in the atmosphere at satellite overpass time and location had passed over a nonmaritime region at some time during the previous 5 days.

[e]MI = Multiangle Imaging Spectroradiometer (MISR); MO = Moderate Resolution Imaging Spectroradiometer (MODIS); AOT: aerosol optical thickness; AR = AERONET.

the MISR and MODIS teams are based on slightly different solar models. MISR uses the model of *Wehrli* [1985], whereas MODIS uses a combination of three models, as described in *Lyapustin et al.* [2007]. In this paper, we retain the E_0 values adopted by the instrument teams for initial comparisons to explore their impact on standard instrument product discrepancies.

[11] We collected colocated MISR and MODIS reflectance measurements from two or three separate patches for each case over cloud-free ocean and, to the extent possible, in close proximity to the AERONET site (Table 3). Each patch is a 3 × 3 array of 1.1 km MISR pixels, along with the associated 1.0 km MODIS pixels whose centers lie within the 3 × 3 MISR array.

[12] To achieve coincidence between the MISR and MODIS observations, we digitally colocated the two data sets using the data product geographic information, reported to be accurate to better than 50 m for both instruments [*Jovanovic et al.*, 2002; *Wolfe et al.*, 2002]. The MISR and MODIS pixels, though closely matched, do not sample identical areas. On the basis of published geolocation accuracy, differences in the MISR and MODIS pixel grids produce edge misalignment no larger than 0.5 km (half the MODIS pixel width). Sun glint contamination is avoided by eliminating any MISR view that either falls within 40° of the Sun's reflection vector from the nominal surface, or is near this value and exhibits patch reflectance variance 3 or more times greater than cameras viewing farther from the Sun glint direction.

[13] Patches were selected within 70 km of the AERONET sites, for which the equivalent reflectance, assessed separately for each spectral band of each MISR view angle not in Sun glint, varied less than about 1% from the patch mean. The spatial uniformity criterion minimizes the contribution scene variability can make to reflectance differences caused by any remaining spatial coverage mismatch. For most events we found at least one patch within 30 km of the AERONET site that met all the selection criteria. The requirement that selected patches fall within the overlap between coincident, successful MISR and MODIS standard retrieval regions contributed to the greater patch distance from the AERONET site in some cases. We relied on back-trajectory analysis from the Hybrid Single-Particle Lagrangian Integrated Trajectory (HYSPLIT) model (R. R. Draxler and G. D. Rolph, 2003, HYSPLIT model access via the NOAA ARL READY Web site, NOAA Air Resources Laboratory, Silver Spring, Maryland, available at http://www.arl.noaa.gov/ready/hysplit4.html, hereinafter referred to as Draxler and Rolph, 2003) (Table 1), MISR-retrieved aerosol characteristics, and the similarity among patch reflectances for each event to build confidence in the assumption that the AERONET and satellite instruments observed the same aerosol air mass. In some cases we relaxed this constraint to achieve greater spatial proximity, as discussed below (e.g., section 3.4).

[14] In addition to the pixel-level equivalent reflectances determined by each instrument, we also made use of the results of the standard aerosol products from both MISR and MODIS. The MISR Standard Aerosol product reports AOT on a 17.6 km grid of 16 × 16 1.1 km pixels and identifies corresponding mixtures of up to three aerosol components, chosen from a predefined set of particle types. The mixtures

Table 2a. MISR, MODIS, and AERONET Spectral Band Information

Band	Effective Wavelength [a], nm	Effective Bandwidth [a], nm	E_0 [b], W/m^2- μm	Spatial Resolution [c], m	Ozone Correction Factor[d]	H_2O Vapor Optical Depth[e]	CO_2 Optical Depth[e]
MISR blue	446.4	41.9	1867.27	275 nadir 1100 off-nadir	5.67×10^{-6}	–	–
MISR green	557.5	28.6	1842.51	275 nadir 1100 off-nadir	1.04×10^{-4}	–	–
MISR red	671.7	21.9	1524.22	275 all cameras	4.89×10^{-5}	–	–
MISR NIR	866.4	39.7	977.755	275 nadir 1100 off-nadir	3.94×10^{-6}	0.002	–
MODIS-3	465.7	18.6	2087.94	500	1.01×10^{-5}	–	–
MODIS-4	553.7	19.7	1865.94	500	9.85×10^{-5}	–	–
MODIS-1	646.3	47.8	1606.17	250	7.86×10^{-5}	see note	–
MODIS-2	856.5	37.7	992.204	250	–	see note	–
MODIS-5	1242.3	23.5	474.344	500	–	see note	4.196×10^{-4}
MODIS-6	1629.4	28.4	240.230	500	–	see note	8.260×10^{-3}
MODIS-7	2114.3	52.4	90.3250	500	–	see note	2.164×10^{-2}
AERONET-1	340	10	–	–	–	–	–
AERONET-2	380	10	–	–	–	–	–
AERONET-3	440	10	–	–	–	–	–
AERONET-4	500	10	–	–	–	–	–
AERONET-5	675	10	–	–	–	–	–
AERONET-6	870	10	–	–	–	–	–
AERONET-7	1020	10	–	–	–	–	–

[a]The effective bandwidths for MODIS and AERONET are full-width at half maximum; for MISR they are 1% to 1% response values. MISR wavelengths and bandwidths are from *Diner et al.* [1998]; for MODIS, they are from *Xiong et al.* [2006]; for AERONET, wavelengths are from the AERONET data files, and bandwidths are from the Cimel CE-318 Sun photometer specification document (http://www.cimel.fr/photo/pdf/ce318_us.pdf). The Ascension Island site reports at 670 nm in the red band instead of the nominal 675 nm. AERONET sky scan measurements include only the 440, 675, 870, and 1020 nm bands [*Dubovik et al.*, 2000]. NIR: near infrared.

[b]E_0 values for MISR are reported in the MISR Standard product. MODIS E_0 values were obtained by averaging the E_0 values given in the MODIS product over each detector within the MODIS band to assure consistent use of the MODIS calibration solar model. (There are 40 detectors for Bands 1 and 2, and 20 detectors for the others [see *Ignatov et al.*, 2005].) Using the MISR Standard *Wehrli* [1985] rather than the MODIS Standard (from three sources for different spectral ranges, as described by *Lyapustin et al.* [2007]) solar model for the MODIS blue band reduces E_0 for this band to 2016.08. Differences in the other bands are at least an order of magnitude smaller.

[c]Spatial resolution is given at satellite nadir for MODIS.

[d]The ozone correction factors were calculated using ozone cross sections for 223 K temperature and 100 hPa pressure, representative of stratospheric conditions, along with the MISR and MODIS band passes shortward of 851 nm from http://www-misr.jpl.nasa.gov/mission/valwork/cal_data/response/profiles.txt and http://www.mcst.ssai.biz/mcstweb/index.html, respectively. For MISR these correction factors take into account recent ozone cross-section measurement improvements [*Bogumil et al.*, 2003], including temperature dependence [*Horváth*, 2004]; they differ by 1.2% and 4% from the values used in the MISR Standard Aerosol Retrieval algorithm (V17 and below) [*Diner et al.*, 1999a; *Kahn et al.*, 2001b] for the green and red bands, respectively, where they are most significant. For MODIS the factors calculated here are larger in the blue and red, and somewhat smaller in the green than those in the Standard algorithm. These factors are multiplied by the column ozone abundance in Dobson units (DU) to give the ozone optical depths (equation (4)).

[e]The water vapor optical depth for MISR is a constant correction applied only to the near infrared band [*Diner et al.*, 1999a]. MODIS CO_2 optical depths, obtained from the MODIS operational code, are also climatological values. The MODIS water vapor optical depth, obtained from the MODIS operational code, is given in terms of the expansion $\tau = G^{-1} \exp\left[k_{\lambda,1} + k_{\lambda,2} \ln(H_2O \times G) + k_{\lambda,3} \ln^2(H_2O \times G)\right]$, where $G\ (=1/\mu + 1/\mu_0)$ is the geometric factor, H_2O is the total column water vapor in centimeters, and the band-dependent k's are defined as in Table 2b.

selected produce simulated TOA equivalent reflectances that compare favorably with the reflectances observed by MISR, on the basis of a set of chi-squared criteria [*Martonchik et al.*, 2002; *Kahn et al.*, 2001a]. Over dark water, only the red (672 nm) and near-infrared (NIR, 866 nm) MISR bands are used for all view angles not in Sun glint; over heterogeneous land (not considered in the present study) the blue and green bands are included as well. The aerosol mixture or mixtures that meet the chi-squared acceptance criteria define the MISR-retrieved range of particle microphysical properties: size, shape, and single-scattering albedo (SSA).

[15] The MISR product reports both the AOT for the mixture that passes all the chi-squared tests and has the lowest chi-squared absolute value (we call this the "lowest-residual" AOT) and a "best estimate" AOT. The best estimate AOT is the arithmetic mean AOT of all the mixtures that meet the acceptance criteria, with each mixture given equal weight. For the current analysis we consider individual mixtures from among those that were accepted to define particle microphysical properties, starting with the one having the lowest residual. When making comparisons with MODIS and AERONET observations, the "MISR atmosphere" refers to a MISR-retrieved best estimate AOT (the MISR AOT product that has been formally validated [e.g., *Kahn et al.*, 2005a] and is most widely used) and associated lowest-residual mixture. This combination is used because a single mixture must be chosen when defining particle properties for each analysis. As needed, we also perform sensitivity analyses on the AOT used.

Table 2b. MODIS Water Vapor Band Correction Factors

Band	k_1	k_2	k_3
MODIS Band 1	−5.73888	0.925534	−0.0188365
MODIS Band 2	−5.32960	0.824260	−0.0277443
MODIS Band 5	−6.39296	0.942186	−0.0131901
MODIS Band 6	−7.76288	0.979707	0.007784
MODIS Band 7	−4.05388	0.872951	−0.0268464

[16] The MODIS Standard Aerosol product reports AOT on a 10 km grid of 10 × 10 1 km pixels, along with a selected coarse and a fine-mode component from a predefined set of each, and the fraction of AOT attributed to the fine mode [*Remer et al.*, 2005; *Levy et al.*, 2005; Remer et al., 2006]. A minimization criterion is used to choose the

Table 3. MISR Patch Summary[a]

Island Site	Date	Patch	Distance to AERONET, km	Latitude[b]	Longitude[b]	AERONET AOT	MISR AOT	MODIS AOT C4	MODIS AOT C5	AERONET SSA	MISR SSA	MODIS SSA C4	MODIS SSA C5
Forth Crete	13 Sep 2003	P1	19.9	35.45	25.45	0.11	0.16	0.13	0.16	0.99	1.00	0.95	0.98
		P2	36.8	35.62	25.47		0.12	0.12	0.14		1.00	0.95	0.98
		P3	56.3	35.80	25.52		0.13	0.11	0.12		0.91	0.95	0.99
Ascension	18 Feb 2005	P1	57.4	−7.64	−14.80	0.21	0.14	0.13	0.15	(0.71)	1.00	0.91	0.96
		P2	53.4	−7.81	−14.86		0.15	0.13	0.14		1.00	0.90	0.96
		P3	55.6	−8.01	−14.90		0.15	0.12	0.13		1.00	0.90	0.96
Ascension	1 Jan 2005	P1	69.6	−7.65	−14.94	0.12	0.12	0.08	0.10	(0.77)	0.84	0.92	0.98
		P2	69.2	−8.03	−15.03		0.13	0.07	0.10		0.84	0.92	0.98
Tahiti	12 Aug 2001	P1	42.4	−17.65	−149.99	0.06	0.20	0.18	0.18	0.99	0.98	0.94	0.96
		P2	32.8	−17.69	−149.88		0.20	0.18	0.18		0.98	0.94	0.96
		P3	23.6	−17.35	−149.62		0.17	0.17	0.18		0.98	0.93	0.96
Tahiti	3 Sep 2003	P1	10.1	−17.47	−149.58	0.05	0.05	0.03	0.05	0.99	0.97	0.90	0.99
		P2	44.8	−17.87	−149.88		0.05	0.01	0.02		0.97	0.88	0.97
		P3	45.9	−17.22	−149.85		0.05	0.01	0.02		0.92	0.88	0.98

[a]All retrieval values are reported at the MISR green band wavelength (557.5 nm), interpolated from the nearest AERONET and MODIS channels linearly in log-log space. SSA: single-scattering albedo.
[b]These are the center latitudes and longitudes of the 3.3 × 3.3 km patches and distances from the center of the 3 × 3 MISR pixel array to the AERONET site.

best-fitting mixture, and the associated AOT is reported. Over water the aerosol retrieval is constrained by observations in six nadir-viewing spectral bands: Band 4 (554 nm), Band 1 (646 nm), Band 2 (857 nm), Band 5 (1.24 microns), Band 6 (1.63 microns), and Band 7 (2.11 microns). To avoid Sun glint, the MODIS Standard Aerosol Retrieval algorithm excludes pixels falling within 40° of the specular direction [*Remer et al.*, 2005].

[17] As with MISR, a "best estimate" AOT is derived from the MODIS results by averaging the retrieved AOT for the three mixtures whose simulated TOA reflectances have the lowest residuals relative to the measured values, or all aerosol mixtures whose residuals fall below 3% [*Remer et al.*, 2005]. We refer to a MODIS-retrieved best estimate AOT and corresponding best-fitting mixture as the "MODIS atmosphere" when making comparisons with MISR and AERONET observations. For comparison purposes we include both Collection 4 and Collection 5 MODIS aerosol retrievals. (A summary of the relevant algorithm differences is posted at http://modis-atmos.gsfc.nasa.gov/products_C005update.html.)

[18] The MISR and MODIS Standard Aerosol Retrieval algorithms over ocean choose pixel-level reflectances used in the retrieval differently and assume different wavelength-dependent water-leaving reflectances (A_0) and near-surface wind speeds. Specifically, MISR selects the darkest pixel that meets the reflectance data quality, deep water, cloud-clearing, spatial correlation, and angular smoothness criteria in the 17.6 × 17.6 km region separately for each channel [*Diner et al.*, 1999a; *Martonchik et al.*, 2002], whereas over each 10 × 10 km region, MODIS truncates the pixels in the lowest and highest 25% of the 857 nm channel reflectance histogram and uses the mean of the middle 50% [*Remer et al.*, 2005]. The effects of these choices are discussed in section 3 below.

[19] The MISR algorithm assumes the water-leaving reflectance, described as an effective Lambertian albedo A_0, to be zero in the red and NIR bands used for the dark water retrieval [*Diner et al.*, 1999b], whereas the MODIS algorithm assumes A_0 to be 0.005 in the 554 nm band and zero in the other bands [*Levy et al.*, 2003]. As employed in the algorithms, these assumptions are thought to be appropriate for dark water. Near-surface wind speed over ocean drives a standard white cap model for both the MISR and MODIS algorithms; MISR uses a 1° × 1° monthly, global climatology to assign wind speed [*Diner et al.*, 1999b], whereas MODIS assumes 6 m/s everywhere [*Levy et al.*, 2003]. In section 3, we assess the effects of these choices quantitatively for the representative events of this study.

[20] Also note that although most MODIS aerosol algorithm changes between Collection 4 and Collection 5 apply to the overland algorithm, the refractive indices for three of the coarse-mode particles used over water were changed for Collection 5 (Remer et al., 2006). This has ramifications in terms of the retrieved AOT, in large part because it changes the retrieved fine/coarse particle ratio. Where relevant, details are given in the examples below (e.g., section 3.3.1), though a comprehensive description and analysis of these issues is being performed separately by the MODIS team.

2.2. AERONET

[21] We use AERONET AOT and particle property retrieval results to constrain a forward radiative transfer model (described in section 2.3 below) that generates TOA equivalent reflectances for comparison with MISR and MODIS values. AERONET Sun- and sky-scanning photometer data for the events of interest were obtained from the program's Web site (http://aeronet.gsfc.nasa.gov). Standard AERONET AOT products were acquired in bands centered at about 340, 380, 440, 500, 675, 870, and 1020 nm (Tables 2a

Table 4. AERONET, MISR, and MODIS Standard Aerosol Retrieval Overview for Individual Events[a]

Island Site	Date	Terra Orbit	Terra Time, UTC	AERONET AOT 558 nm	MISR AOT 558 nm	MODIS AOT 558 nm	AERONET Ångstrom Exponent	MISR Ångstrom Exponent	MODIS Ångstrom Exponent	AERONET Skyscan Time, UTC	AERONET SSA[b], 558 nm	MISR SSA[b], 558 nm	MODIS SSA[b], 558 nm
Forth Crete	13 Sep 2003	19878	0904	0.11	0.13	0.13	2.01	1.50	1.30	0917	0.99	0.96	0.98
Ascension	18 Feb 2005	27510	1119	0.21	0.15	0.14	0.28	1.03	0.19	0935	(0.71)	1.00	0.96
Ascension	1 Jan 2005	26811	1119	0.12	0.12	0.10	0.64	1.21	0.75	1103	(0.77)	0.84	0.98
Tahiti	12 Aug 2001	8788	2022	0.06	0.18	0.18	0.57	0.48	0.48	2106[c]	0.99	0.98	0.96
Tahiti	3 Sep 2003	19739	2014	0.05	0.05	0.03	1.09	0.94	2.07	2001[c]	0.99	0.95	0.98

[a]For qualitative comparison, AERONET AOT and SSA are interpolated logarithmically to the MISR green band effective wavelength (557.5 nm) using the two nearest AERONET channels, usually 500 nm and 675 nm. (Quantitative comparisons are accomplished using the forward radiative transfer model, run at the effective wavelength appropriate to each instrument.) The AERONET values reported are from the available measurements closest in time to the Terra overpass (usually within 15 min). MODIS AOT and SSA are interpolated linearly to 557.5 nm in log-log space from the two nearest MODIS bands, 553.7 nm and 646.3 nm. The MODIS Ångstrom exponent is derived for the wavelength range 550 to 865 nm, as reported in the MODIS Standard product. MISR and MODIS Standard product AOT and particle property values are averages with equal weight of those reported for the selected patches (see Tables 2a and 2b), except Forth Crete, which uses only P2 and P3. SSA is reported for the ''best fitting'' and ''lowest-residual'' aerosol particle models for MODIS and MISR, respectively. Results given here are for the MISR Standard Aerosol product V17, MODIS Standard Aerosol product Collection 5, and AERONET Level 2.0.

[b]AERONET SSA retrievals are not considered reliable when the AOT at 440 nm falls below 0.4 [*Dubovik et al.*, 2000], as it does for all the cases in this study. There is little information about SSA from MISR for the low AOTs in these cases either [e.g., *Kahn et al.*, 2001a], and for MODIS they are essentially assumed here as well [e.g., *Remer et al.*, 2005]. These values are nevertheless included in this table for comparison purposes, since the MISR- and MODIS-retrieved AOTs depend in part on the SSA adopted in the retrieval (see section 2.2).

[c]For the Tahiti cases, the AERONET sky scan retrievals are reported as ''not Level 2, use with caution'' (S. Smirnov, personal communication, 2006). However, the AERONET direct Sun measurements are reported as nominal.

and 2b), along with column water vapor, as frequently as every 15 min under cloud-free, daylight conditions from direct Sun observations. In each case we used the measurements closest in time to the Terra overpass, but also considered all successful 15 min AOT results taken within ±1 hour of the Terra overpass in the discussion, to help account for spatial variability in the satellite retrieval region. In general, we expect AOT over ocean to vary little over tens-to-a-few-hundred-kilometers spatial scales [e.g., *Smirnov et al.*, 2002; *Anderson et al.*, 2003], so point aerosol measurements are often treated as representative of larger areas. Interesting exceptions are discussed in section 3.2 below. Ångstrom exponents were calculated as the negative slope in log-log coordinates of a least squares fit to the AERONET AOT values, interpolated to the four MISR wavelengths, in the spectral range 446 to 866 nm.

[22] V2 AERONET products are used in this study. The AERONET direct Sun measurements are primarily Level 2, for which full quality control has been performed, including cloud screening that relies on AOT variability among three direct Sun observations taken 1 min apart on each 15 min measurement center, and before-and-after radiometric calibration [*Smirnov et al.*, 2000]. Level 2 direct Sun AOT retrievals are generally believed to be accurate to about 0.02 for midvisible wavelengths.

[23] Table 4 summarizes the AERONET AOT for each event, interpolated linearly to the centroid of the MISR green channel (558 nm), using the two AERONET channels nearest in wavelength. AERONET AOT values for the other MISR and MODIS bands were determined the same way. The AOT variability was within about 0.005 for all the cases considered here. The AERONET AOT uncertainties, given as whiskers in subsequent figures, represent measurement ranges over the averaging period.

[24] The AERONET instruments are also programmed to perform sky scans in the principal plane and across the almucantar at 440, 670, 870, and 1020 nm about once per hour, from which aerosol size distributions and SSA are derived [*Dubovik and King*, 2000; *Dubovik et al.*, 2002]. This process is independent of the 15 min AOT retrievals, which are obtained from direct solar transmission, calibrated using the Langley method [*Holben et al.*, 1998].

[25] The highest-quality particle property retrievals are obtained for solar zenith angles greater than 45° and for AOT (at 440 nm) greater than about 0.4 [*Dubovik et al.*, 2000]. Since low AOT values (Table 4) and, in some cases, small solar zenith angles (Table 1) are of interest in the present study, we selected specific sky scan instances as close in time as possible to the MISR overpasses, for which the algorithm performed well and retrieved reasonable particle size distributions, on the basis of the experience of the AERONET team (A. Smirnov, personal communication, 2006). Although these observation times were less closely matched than for the AOT data, they were often less than 30 min. The longest period between the satellite overpass and sky scan is just under 2 hours, for Ascension Island on 18 February 2005 (Table 4), discussed in section 3.2.

[26] Retrieved size is reported as relative volume-weighted amount in 22 bins of particle radius, spread logarithmically between 0.05 and 15 microns. Size distributions are also provided in the AERONET Standard product as one medium-mode and one coarse-mode lognormal parameter fit to the 22 bin histogram [*Dubovik and King*, 2000]. A combination of direct Sun and sky scan data is used to retrieve spectral indices of refraction and SSAs, though they are considered reliable only when the AOT at 440 nm is 0.4 or above [*Dubovik et al.*, 2000]. We nevertheless include the AERONET SSA values in Table 4 for comparison purposes, since scattered light is used to retrieve extinction AOT for MISR and MODIS, and the AOT values reported by those

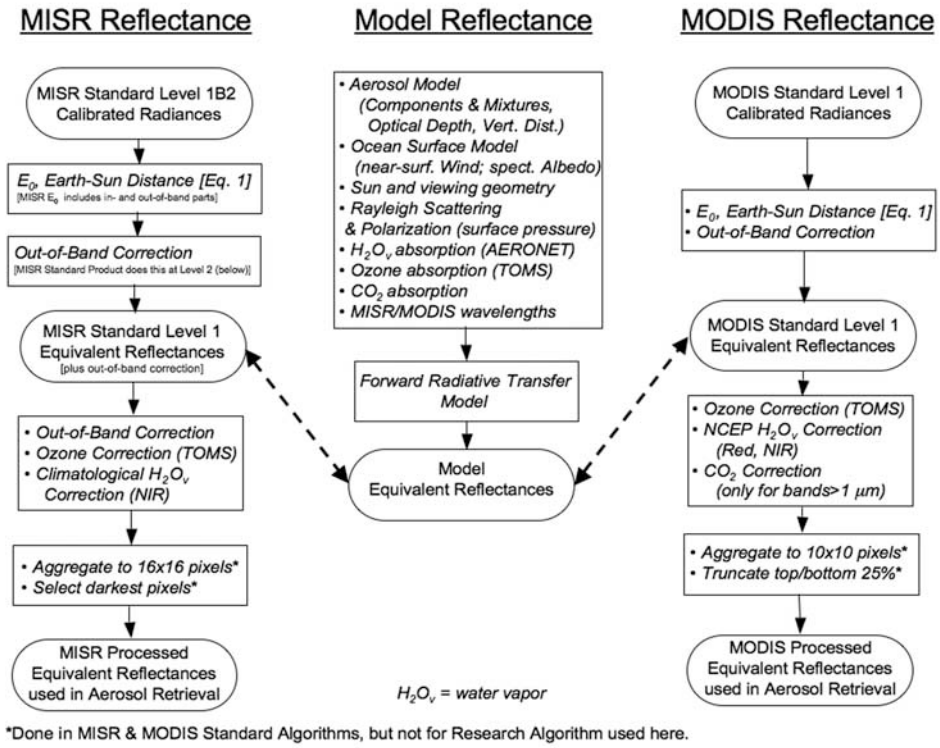

Figure 1. Multiangle Imaging Spectroradiometer (MISR)–Moderate Resolution Imaging Spectroradiometer (MODIS) reflectance comparison data processing flow chart, summarizing the steps taken to produce MISR, MODIS, and model equivalent reflectances used for direct comparison and for aerosol retrieval analysis in this study.

instruments depend on the aerosol SSA and size distributions used by their retrieval algorithms.

[27] Also shown in Table 4 are representative MISR and MODIS AOT and aerosol property values derived from the standard products. The MODIS product does not explicitly provide an SSA value for the retrieved bimodal aerosol mixture. The values given in Table 4 were calculated by first finding the ratio of the small to large particle number density for the best-fitting MODIS model. Because the AOT, represented by τ_λ in equation (2) below, is defined as the product of the aerosol extinction cross section, C_{ext}, and the column-integrated number density, N, we can write the ratio of the small to large particle numbers as

$$\frac{N^s}{N^l} = \frac{\tau_\lambda^s}{\tau_\lambda^l}\frac{C_{ext,\lambda}^l}{C_{ext,\lambda}^s}, \tag{2}$$

where the superscripts s and l refer to the small and large particle modes, respectively. The effective SSA for the bimodal distribution, represented by $\varpi\lambda$ in equation (3), is given by the relation

$$\varpi_\lambda = \frac{\left(\frac{N^s}{N^l}\right)C_{ext,\lambda}^s\varpi_\lambda^s + C_{ext,\lambda}^l\varpi_\lambda^l}{\left(\frac{N^s}{N^l}\right)C_{ext,\lambda}^s + C_{ext,\lambda}^l}. \tag{3}$$

2.3. Radiance Data Processing and Forward Modeling

[28] The approach adopted here is similar to that used by *Kahn et al.* [2005b], where a forward radiative transfer model, constrained by AERONET observations, produces TOA equivalent reflectances at the MISR and MODIS view angles and effective wavelengths, making direct comparisons possible. Since the present study is aimed at understanding the MISR and MODIS Level 2 aerosol retrievals, we subsequently take the further step of constraining the forward model with each of the MISR atmosphere and MODIS atmosphere results. Figure 1 summarizes the (Level 1) MISR and MODIS radiance and equivalent reflectance processing steps needed as input to the (Level 2) standard and the MISR Research Aerosol Retrieval algorithms. At the level of detail relevant here, the main differences between the MISR and MODIS data streams are as follows: (1) The correction for out-of-band response is included in the MODIS Standard Level 1 reflectance product, whereas for MISR it is performed in the Level 2 aerosol retrieval code. (2) The water vapor correction is done on the basis of a climatology for MISR, whereas for MODIS the NCEP analysis model output is used. (3) The Standard Level 2 aerosol algorithms take different approaches for selecting and aggregating pixel-level reflectance data [*Martonchik et al.*, 2002; *Diner et al.*, 1999a; *Remer et al.*, 2005; and references therein]. For the MODIS long-wave bands a CO_2 correction is made as well.

[29] To test consistency of the retrieved Level 2 MISR and MODIS aerosol products, we also explicitly performed the Rayleigh scattering and polarization, ozone, water vapor, and CO_2 corrections in model simulations of the Standard Level 1 products, and for MISR the out-of-band correction as well [e.g., *Kahn et al.*, 2001b]. For both MISR and MODIS the spectral Rayleigh scattering formula given by *Russell et al.* [1993] was used with the observed surface pressure (Table 1) to calculate this contribution. The MODIS Standard Retrieval algorithm uses the Rayleigh-scattering formula from *Gordon et al.* [1988], based on *Hansen and Travis* [1974], but except for the three MODIS long-wave channels, the differences are less than 0.34% even when N_2, O_2, Ar, and CO_2 are all explicitly included. These differences are negligible for our purposes. The polarization correction for both instruments was accomplished by multiplying the Rayleigh-scattering contributions in all bands by a factor that accounts for the reduced TOA radiance when a vector rather than a scalar radiative transfer algorithm is used [e.g., *Kattawar et al.*, 1976]. Instrument sensitivity to polarization itself is reported as <1% for MISR [*Diner et al.*, 1999b] and <2% for MODIS [*Kaufman et al.*, 1997]; the vector algorithm used here is based on *Evans and Stephens* [1991].

[30] For ozone, MISR water vapor, and MODIS CO_2 the corrections amount to calculating effective absorption spectral optical depths $\tau_{g,b}$, using constraints on the gas column amount A_g and band-specific conversion factors $F_{g,b}$:

$$\tau_{g,b} = F_{g,b} \times A_g, \tag{4}$$

where subscript g indexes the gas type and b indexes the instrument spectral band. Ozone and water vapor column amounts used in each case are given in Table 1, and band-specific E_0 and gas absorption correction factors are detailed in Tables 2a and 2b. The MODIS water vapor correction is described in the notes for Table 2a.

[31] In section 3, we compare the MISR and MODIS equivalent reflectances with results from the forward model, as indicated by the heavy dashed arrows in Figure 1. AOT differences are examined subsequently in light of these comparisons. The radiative transfer model used to link the MISR and MODIS observations is described in detail and validated against other radiative transfer models in previous work [*Martonchik et al.*, 1998; *Kahn et al.*, 2005b]. In brief, as with the MISR Standard Aerosol Retrieval algorithm, the model is based on an adding-doubling approach using the *Grant and Hunt* [1968] method, with the ocean surface represented as a Fresnel reflector with a wind-speed-dependent whitecap model [*Cox and Munk*, 1954; *Koepke*, 1984] and wavelength-dependent water-leaving reflectance (A_0). Typical dark water values of A_0, abstracted from *Morel and Maritorena* [2001], are 0.03, 0.007, 0.002, and 0.0007 in the MISR blue, green, red, and near-infrared bands, respectively, and 0.0 in the longer-wavelength MODIS bands.

3. MISR-MODIS-AERONET AOT Comparisons

[32] We now delve into events selected to cover the most widely observed MISR, MODIS, and AERONET AOT discrepancies with the aim of learning as much as we can about their root causes. Bear in mind that there are vastly more cases that do not exhibit such differences, but when aggregates of the product are used for climate studies, these differences sometimes matter. Here we systematically analyze the aggregated information about reported equivalent reflectance, surface treatment, adopted aerosol optical properties, and observed variability for each case.

3.1. Forth Crete, 13 September 2003: Water-Leaving Reflectance and Particle-Type Retrievals

[33] Figure 2a shows the grids of standard MISR 17.6 km, relatively cloud-free ocean retrieval regions (green; centers marked with green pluses), and MODIS standard 10 km retrieval regions (white; centers marked with white crosses), as well as the study patches used for detailed reflectance comparisons and research retrievals (yellow diamonds). The AERONET site is located toward the eastern side of Crete's north coast (red triangle near the bottom left of the image). Figure 2b is a plot of the best estimate and lowest-residual spectral AOT derived by the MISR and MODIS Standard algorithms for the retrieval regions that contain the three patches (Table 3 and Figure 2a). AERONET spectral AOT averages for three measurements taken 15 min apart around Terra overpass time are shown as red triangles; whiskers indicate the AERONET-observed AOT range over approximately ±1 hour, centered on the overpass. The AOT for this event is above 0.1 in the green band (557.5 nm for MISR and 553.7 nm for MODIS), moderately high for an ocean case. On the basis of HYSPLIT back-trajectories (Draxler and Rolph, 2003) the near-surface air mass traveled over the eastern Mediterranean for the previous 24 hours, and over the previous 5 days, came from the west and north. This suggests possible continental influence, though the midvisible SSAs adopted by MISR and MODIS are 0.96 or higher (Table 4), and AERONET reports SSA of 0.99 across the visible spectrum. We investigate several aspects of Figure 2b: (1) the spread in AOT values among the three patch locations, (2) the systematic differences between the MISR, MODIS, and AERONET AOT magnitudes and slopes, and (3) differences between the "best estimate" (from MISR and MODIS), "lowest-residual" (for MISR), and "best fit" (for MODIS) results.

3.1.1. Patch AOT and Nadir Reflectance Differences

[34] For both MISR and MODIS the patch P1 AOT is higher than that of the other patches at all wavelengths by as much as 0.04 for MISR and MODIS C5, and 0.03 for MODIS C4 in the midvisible. The difference is larger than the average uncertainty reported by either instrument over dark water, is systematic across wavelengths, angles, locations, and instruments (Figure 2), and is of interest because this is an especially clean, apparently cloud-free case. The patch P2 and P3 spectral AOTs agree with each other to well within expected measurement uncertainties. (For MODIS C4 and C5, patch P3 is lower than P2 by about 0.01 from the green to the near-infrared bands, and for MISR the patch AOTs are coincident for the red band, but have different spectral slopes, so patch P3 is higher by about 0.01 in the green and lower by about that amount in the NIR.)

[35] For the MISR nadir and MODIS green, red, and NIR channels, Figure 2c indicates that actual variability within

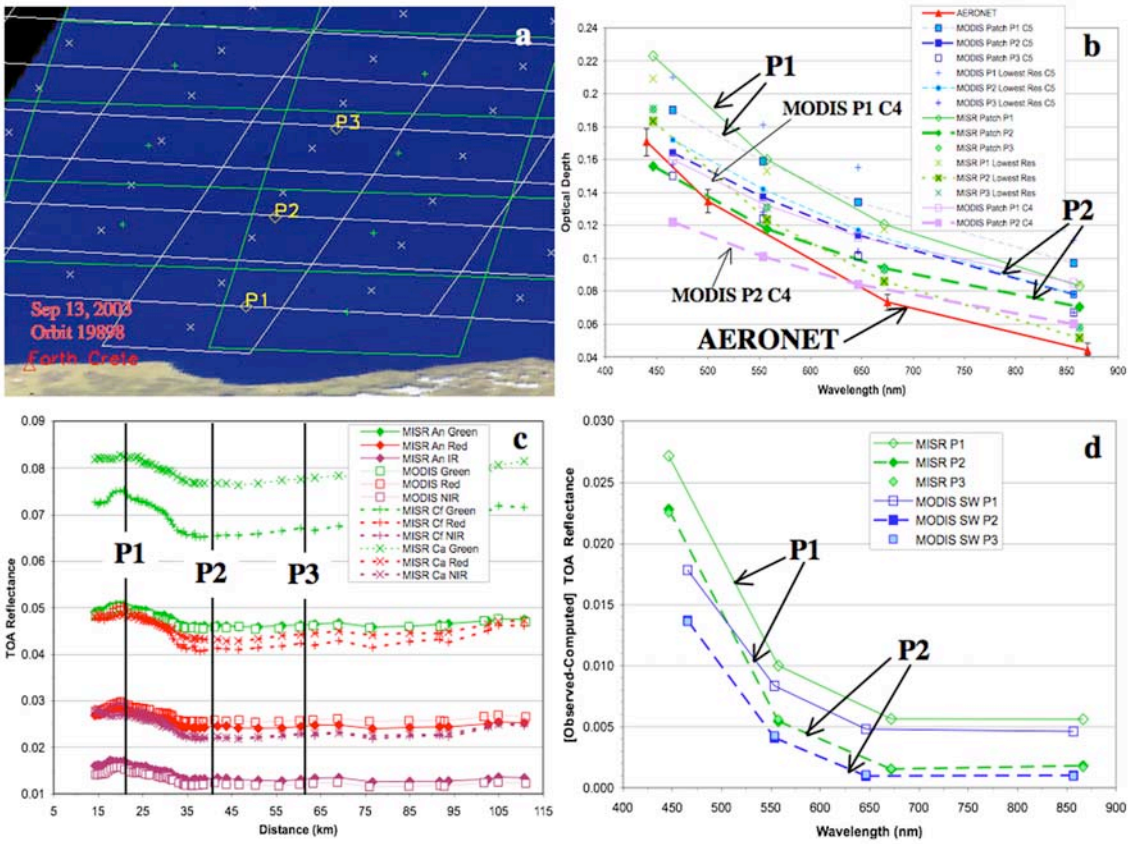

Figure 2. Aerosol optical thickness (AOT) and nadir reflectance analysis for the 13 September 2003 Forth Crete event. (a) MISR nadir camera natural color view of the northeast coast of Crete and surrounding ocean. Superposed on the image are the locations of the MISR 17.6 km (green boxes) and the MODIS 10 km (white boxes) aerosol standard retrieval regions and the Aerosol Robotic Network (AERONET) site location (red triangle). Three 3 × 3 km study patches for this event are indicated with yellow diamonds. (b) Best estimate MISR (green diamonds) and MODIS (blue squares) and lowest-residual (green crosses and blue pluses) standard Collection 5 (C5) aerosol product spectral AOT values plotted against band effective wavelength for retrieval regions containing patches P1, P2, and P3 (Figure 2a and Table 3). The MODIS Collection 4 (C4) AOT values for P1 and P2 are plotted in purple. The AOT points for patch P1 are connected with thin solid lines, and for patch P2 they are connected with dashed lines, to aid interpretation. Mean AERONET AOT values for three measurements taken 15 min apart around Terra overpass time are given as red triangles, connected by a solid line; whiskers represent the AOT range within approximately ±1 hour of overpass. (c) MISR nadir (An), 60° forward (Cf), 60° aft (Ca), and MODIS green, red, and near-infrared (NIR) channel top of atmosphere (TOA) equivalent reflectance values along a traverse that extends northward from the edge of MISR/MODIS joint coverage near the coast (Figure 2a) nearly linearly through P1, P2, and P3, and continuing NNE about 50 km further across the Mediterranean. (d) Differences between MISR nadir or MODIS observed TOA reflectances and model values for three patches in four spectral bands, each evaluated and plotted at the effective wavelength of the observation. The model assumes the AERONET-derived AOT and particle properties (Table 4), the observed surface pressure and wind speed (Table 1), and as in the standard satellite retrieval algorithms, $A_0 = 0$ except for the MODIS green band, where it is 0.005. The patch P1 and P2 MISR and MODIS points are connected with straight lines to aid interpretation. Note that the blue band observations, which are not used in either the MISR or MODIS aerosol retrievals, contain a large contribution from the ocean surface that is not included in the models.

the scene can account for the retrieved AOT differences between patch P1 and patches P2 and P3. Figure 2c shows equivalent reflectances along a traverse starting near the coast, going northward almost linearly through all three patches and continuing NNE about 50 km further into the Mediterranean. Patch P1, about 20 km from the coast, is at a subtle reflectance peak, approximately 0.005 in magnitude at all three wavelengths, which amounts to about 10%, 20%, and 30% in the green, red, and NIR bands, respectively.

[36] This gray addition to the scene reflectance may be due to extremely thin cloud or perhaps some spectrally neutral, large-sized aerosol in the atmosphere, local

Table 5. AERONET, MISR-, and MODIS-Retrieved Aerosol Mixture Overview[a]

Island Site	Date	Terra Orbit	Terra Time, UTC	Patch	AERONET Fine Mode			AERONET Coarse Mode			MISR Mix	MISR Particle 1			MISR Particle 2			MISR Particle 3			MODIS Fine Mode			MODIS Coarse Mode		
					τ%	r_{eff}	σ	τ%	r_{eff}	σ		τ%	r_{eff}	σ	τ%	r_{eff}	σ	τ%	r_{eff}	σ	τ%	r_{eff}	σ	τ%	r_{eff}	σ
Forth Crete	13 Sep 2003	19878	0904	P2	82	0.14	1.45	18	2.0	1.83	11	100	0.12	1.7	–	–	–	–	–	–	74	0.15	1.82	26	1.98	1.82
											63	40	0.12	1.7	48	0.75	1.5	12	3.32	2.0	**89**	**0.20**	**1.82**	**11**	**1.98**	**1.82**
Ascension	18 Feb 2005	27510	1119	P2	52	0.17	1.72	48	1.7	2.10	8	40	0.056	1.65	60	2.8	1.9	–	–	–	28	0.10	1.49	72	1.98	1.82
																					17	**0.10**	**1.49**	**83**	**1.98**	**1.82**
Ascension	1 Jan 2005	26811	1119	P1	57	0.14	1.65	43	1.9	2.10	33	10	2.8	1.9	90	0.12	1.7	–	–	–	42	0.10	1.49	58	1.98	1.82
											34	20	2.8	1.9	80	0.12	1.7	–	–	–	**59**	**0.20**	**1.82**	**41**	**1.98**	**1.82**
											43	10	2.8	1.9	90	0.12	1.7	–	–	–						
											RESRCH	15	0.1	1.49	40	0.15	1.82	45	1.48	1.82						
Tahiti	12 Aug 2001	8788	2022	P3	49	0.12	1.61	51	2.2	1.99	60	18	0.12	1.7	2	2.8	1.9	80	0.75	1.5	49	0.15	1.82	51	1.98	1.82
																					21	**0.10**	**1.49**	**79**	**1.98**	**1.82**
Tahiti	3 Sep 2003	19739	2014	P1	73	0.17	1.95	27	2.4	1.71	64	40	0.12	1.7	36	0.75	1.5	24	3.32	2.0	24	0.15	1.82	76	1.98	1.82
																					100	**0.20**	**1.82**	**0**	**1.98**	**1.82**

[a]Results given here are for the MISR Standard Aerosol product V17, MODIS Standard Aerosol products, Collections 4 and 5, and AERONET Level 2.0, except the AERONET result for the Tahiti cases (see Table 4). Note that τ% for MISR and MODIS are given at their respective green band effective wavelengths. The MODIS Collection 5 values are shown in bold below the Collection 4 values in the MODIS fine- and coarse-mode columns; for AERONET the fine- and coarse-mode values are for the good quality, V2, Level 1.5 sky scan retrievals closest in time to the Terra overpass (less than 1 hour for all cases except Ascension 18 February 2005, where the time difference is 1 hour 54 min), and τ% is interpolated from the nearest available bands (typically 440 and 675 nm) to 558 nm for comparison purposes. The σ is the lognormal characteristic width, which is sometimes reported as the natural log of the number given here [e.g., *Remer et al.*, 2005]. RESRCH is a mixture created in the MISR Research Aerosol Retrieval algorithm that is not one of the numbered mixtures used by the MISR Standard Aerosol algorithm.

increases in the water-leaving reflectance (A_0), or reflection from a shallow ocean bottom. In fact, the water depth falls to 200 m about 10 km off the coast, so the ocean bottom is unlikely to make a significant contribution to these patches. Also plotted in Figure 2c are the green, red, and NIR TOA reflectances along the traverse for the MISR 60° forward (Cf) and 60° aft-viewing (Ca) cameras. Because of increased atmospheric path length overall, the C-camera reflectances in each spectral band are higher than those in the corresponding nadir bands for the entire traverse. However, the spectral reflectance differences at P1 do not increase systematically with steeper MISR view angle, as would be expected if atmospheric aerosol loading or cloud were viewed through increasing path lengths at the P1 site. We conclude that the P1 reflectance enhancement is likely due to larger water-leaving reflectance. We explore subsequently the magnitude of A_0 required to account for this possibility.

[37] Figure 2c also shows that in this case the MISR nadir reflectances are just slightly, though remarkably systematically, 0.0006, or about 0.01% higher than those of MODIS in the green channel, and 0.001, or about 10% in the NIR, but 0.0014, or about 0.06% lower in the red (MODIS Band 1). Spectral band-pass differences may account for the lack of coincidence, so we use the forward radiative transfer model discussed in section 2.3 to solve for the expected TOA reflectance in each MISR and MODIS spectral band separately, using self-consistent atmospheric and surface assumptions.

[38] In Figure 2d we plot the differences between the measured TOA equivalent reflectances and forward model simulated values (dashed arrows in Figure 1) for the three study patches. For this comparison the model was run with the AERONET-retrieved AOT and particle properties (Tables 4, 5, and 6), near-surface wind speed of 3.6 m/s (Table 1), and the spectral surface reflectance (A_0) values assumed in the standard retrieval algorithms (zero in all bands except the MODIS green; see section 2.1). For reference, the absolute TOA equivalent reflectances in the nadir blue, green, red, and NIR bands are about 0.12, 0.045, 0.025, 0.01, respectively (Figure 3a). Also note that although the blue band is included in Figure 2d, neither the MISR nor the MODIS dark water aerosol algorithms use the reflectance from this band in their retrievals, due in large part to A_0 uncertainties, and to higher absorbing-aerosol vertical distribution sensitivity in the blue band. (The MISR Standard Aerosol Retrieval, V20 and below, does not use the green band either, though later releases of the product may use this band, retrieving a self-consistent constraint on the shorter-wavelength A_0 values.)

[39] In all cases the measured equivalent reflectances are higher than those of the model by amounts that generally decrease with increasing wavelength. MISR appears to be higher than MODIS in each spectral band, even when band-pass spectral location is taken into account. For patches P2 and P3 the MISR green and NIR bands are about 15% above the nominal model, and the corresponding MODIS bands are about 10% above the model. For the red bands the percent differences for MISR and MODIS are about half their respective green values. As expected, for patch P1 the discrepancies between the observations and the nominal model are larger. For MISR the patches P2 and P3 differences map to a 0.01 and 0.02 discrepancy with AERONET AOT in the green and red bands, respectively. Any reduc-

Table 6. MISR and MODIS Component Particle Properties

Component Name	r_1, μm	r_2, μm	r_c, μm	r_e, μm	σ	SSA (446)	SSA (558)	SSA (672)	SSA (866)	SSA (1242)	SSA (2114)	AOT(446)/ AOT(558)	AOT(672)/ AOT(558)	AOT(867)/ AOT(558)	AOT(1242)/ AOT(558)	AOT(2114)/ AOT(558)	g (558)	Particle Size/Shape Category
spherical_nonabsorb_0.06	0.001	0.4	0.03	0.056	1.65	1.00	1.00	1.00	1.00	1.00	1.00	1.95	0.55	0.23	0.05	0.00	0.35	very small spherical
spherical_nonabsorb_0.12	0.001	0.75	0.06	0.12	1.7	1.00	1.00	1.00	1.00	1.00	1.00	1.55	0.66	0.35	0.12	0.02	0.61	small spherical
spherical_nonabsorb_2.80	0.1	50.0	1.0	2.8	1.9	1.00	1.00	1.00	1.00	1.00	1.00	0.99	1.03	1.06	1.12	1.23	0.78	large spherical
spherical_absorb_0.12_ ssa_0.9	0.001	0.75	0.06	0.12	1.7	0.91	0.90	0.89	0.85	0.77	0.53	1.50	0.68	0.37	0.15	0.04	0.61	small spherical absorbing
spherical_absorb_0.12_ ssa_0.8	0.001	0.75	0.06	0.12	1.7	0.82	0.80	0.77	0.72	0.60	0.34	1.47	0.69	0.40	0.17	0.05	0.61	small spherical very absorbing
grains_mode1_h1	0.1	1.0	0.5	0.75	1.5	0.92	0.98	0.99	1.00	NA	NA	0.90	1.06	1.08	NA	NA	0.71	medium dust
spheroidal_mode2_h1	0.1	6.0	1.0	3.32	2.0	0.81	0.90	0.97	0.98	NA	NA	0.99	1.02	1.05	NA	NA	0.77	coarse dust
modis_model_1_small_ 0.10_wet_water_soluble	0.0072	0.49	0.07	0.10	1.49	0.98	0.97	0.96	0.94	0.88	0.50	1.72	0.60	0.28	0.09	0.02	0.51	small spherical
modis_model_2_small_ 0.15_wet_water_soluble	0.0018	1.0	0.06	0.15	1.82	0.98	0.98	0.98	0.97	0.96	0.82	1.40	0.72	0.43	0.18	0.03	0.66	medium spherical
modis_model_3_small_ 0.20_water_soluble_ with_humidity	0.0023	1.33	0.08	0.20	1.82	0.99	0.99	0.98	0.98	0.98	0.92	1.32	0.75	0.48	0.22	0.05	0.72	medium spherical
modis_model_6_C5_ large_1.48_wet_sea_salt	0.018	10.0	0.6	1.48	1.82	0.96	0.97	0.98	0.98	0.99	0.99	0.96	1.04	1.09	1.12	0.93	0.79	medium-large spherical
modis_model_7_C4_ large_1.98_wet_sea_salt	0.023	13.3	0.8	1.98	1.82	0.86	0.88	0.89	0.92	0.94	0.97	0.98	1.03	1.07	1.16	1.12	0.79	large spherical Collection 4
modis_model_7_C5_ large_1.98_wet_sea_salt	0.023	13.3	0.8	1.98	1.82	0.95	0.96	0.97	0.98	0.98	0.99	0.97	1.04	1.09	1.16	1.12	0.80	large spherical Collection 5

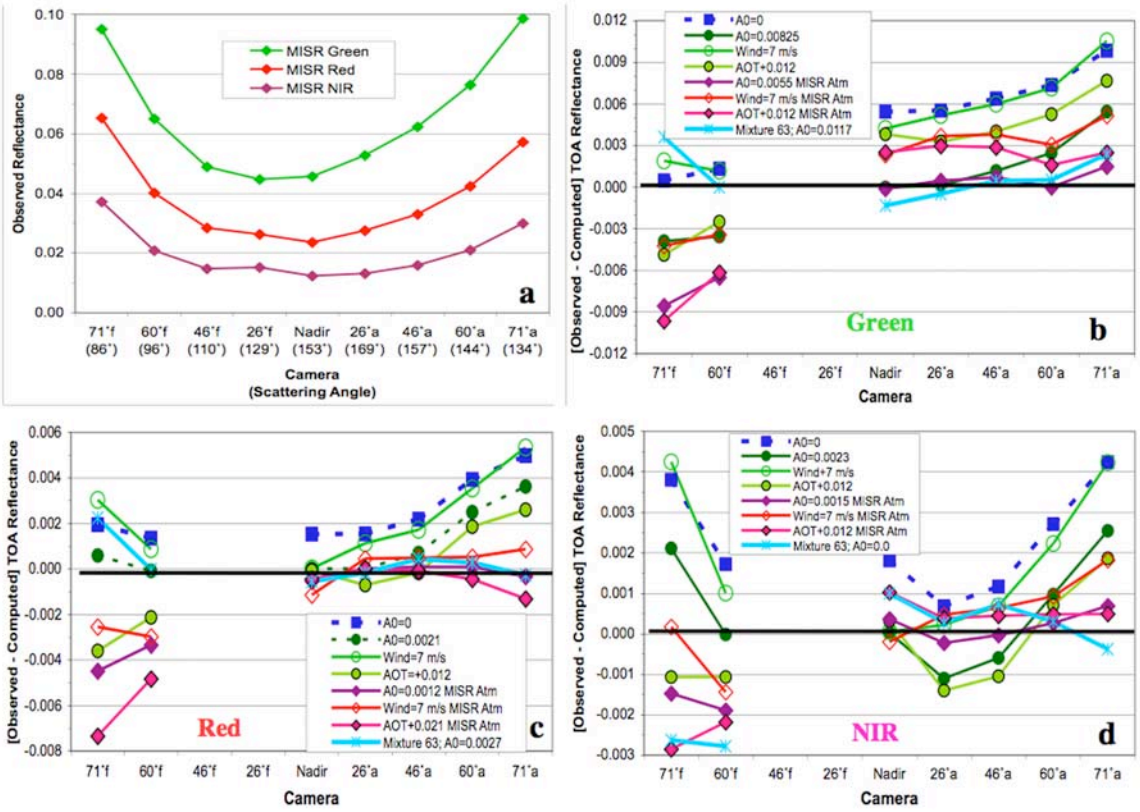

Figure 3. Multiangle reflectance analysis for the 13 September 2003 Forth Crete event, patch P2. (a) MISR-observed TOA equivalent reflectances for the green, red, and NIR bands; the scattering angles for each camera are given below the camera names in the axis label. (b) Green band (observed – modeled) TOA reflectance differences for eight model runs and all MISR cameras not in glint. (c) Same as for Figure 3b, but for the red band. (d) Same as for Figure 3b, but for the NIR band. The nominal AERONET particle properties were used for the first four runs, for the subsequent three runs, the ''MISR atmosphere'' is MISR-retrieved mixture 11 (the ''lowest-residual'' case), and the final run adopts MISR-retrieved mixture 63. In each difference plot, eight separate cases are shown and are listed sequentially in the legend. (1) Dark blue squares indicate reflectance differences for the nominal case: model initialized with $A_0 = 0$, near-surface wind speed 3.6 m/s, midvisible AOT = 0.116, and measured column water vapor and ozone (Table 1). (Observed – modeled) TOA reflectance differences are also shown with the nominal values for all input quantities except (2), (4), and (8), adjusted spectral A_0; (3) and (6), adjusted near-surface wind speed; (4) and (7), adjusted AOT. The adjustments aimed to produce good fits for the nadir camera in the MISR red band and for spectral A_0, each band separately. Straight lines connect the data points to aid interpretation.

tion in the MISR-MODIS ~3% absolute spectral calibration difference in the midvisible, and/or a larger correction in the blue and a smaller one in the near infrared [e.g., *Lyapustin et al.*, 2007; *Bruegge et al.*, 2003], would bring the two into closer agreement with each other. A reduction in the MISR calibration would also improve midvisible AOT agreement with AERONET. However, in this case, likely calibration adjustments would still not completely resolve the differences with the nominal AERONET-driven model. We therefore consider the possible influences of other factors in section 3.1.2.

3.1.2. Multiangle Reflectance Comparisons

[40] We use MISR's multiangle information along with the forward radiative transfer model to test the effects on the model-measurement discrepancies of adjusting spectral A_0, wind speed, and AOT used in the model. For clarity we aim to bring the nadir camera at each wavelength into agreement with the model using the spectral A_0 adjustment, and the nadir red band using the wind and AOT adjustments, which are not spectrally dependent. We then study the agreement among the other channels. Figure 3 shows the effects of these adjustments for the patch P2 observations, assuming either AERONET-retrieved particle properties or MISR-retrieved particle properties. (Note that a separate panel for the blue band is not included in Figure 3 since this band is not actually used in either the MISR or MODIS overwater aerosol retrievals.)

[41] As may be expected on the basis of Figure 2d, in Figures 3b–3d the measurements are brighter in all cameras and bands when $A_0 = 0$ and the AERONET atmosphere is used (dark blue curves). When the AERONET atmosphere is adopted in the model, the spectral A_0 values required to

Table 7. Adjusted Forth Crete Model Spectral Water-Leaving Reflectances (A_0) for Patches P1 and P2[a]

	MISR Nadir P1	MODIS SW P1	MISR Nadir P2	MODIS SW P2	MISR Nadir MISR Atmosphere (M11); P2	MISR Nadir MISR Atmosphere (M63); P2	"Typical" Dark Water
Blue	0.045	0.028	0.038	0.022	0.034	0.047	0.030
Green	0.015	0.013	0.008	0.006	0.006	0.012	0.007
Red	0.008	0.007	0.002	0.002	0.001	0.003	0.002
NIR	0.007	0.006	0.002	0.002	0.002	0.000	0.001

[a]These are the A_0 values required to bring the model and top of atmosphere measurement into agreement for the MISR nadir and MODIS short-wave (SW) channels. For the wind speed and AOT adjustments the nadir red channel differences are minimized. The AERONET atmosphere and average measured wind (Tables 1 and 4) are used to constrain the model in all cases except where "MISR atmosphere" is indicated in the column heading; M11 gives values for the lowest-residual mixture 11, whereas M63 is a multiangle fit using MISR mixture 63 (see Figure 3). Typical dark water A_0 values are given in the last column.

bring the model TOA equivalent reflectances into agreement with the patch P2 MISR nadir and MODIS values are close to the "typical" dark water values mentioned in section 2.3; the A_0 results are summarized in Table 7. For the brighter patch P1 the surface reflectance needed is 0.015 in the MISR green band, about twice the patch P2 value, and 0.0078 in the red, about 4 times the patch P2 value. The required MODIS A_0 values are a little smaller. However, from Figure 3 the angular shape defined by the MISR off-nadir cameras does not fit well when the nominal (AERONET) atmosphere is used. Note that the NIR nadir camera may be affected by some surface scattering; the glint angle is about 46° for this camera, which is outside the expected glint cone, especially for low-to-moderate wind speed, but the reflectance values are barely 0.01 in this channel (Figure 3a), and any small surface effect could scatter light and skew the TOA reflectance. The wind and AOT adjustments shown in Figure 3 (green curves) are not spectrally dependent and produce poor results from band to band and camera to camera with the AERONET atmosphere.

[42] Using the MISR atmosphere with the lowest-residual mixture (mixture 11) in the model, spectral A_0 values required to produce agreement with the MISR nadir camera TOA reflectances are close to the nominal dark ocean values (Table 7), and the angular shape for the aft-viewing cameras is closer to that observed (i.e., the differences plotted are closer to zero) than with the AERONET atmosphere (Figures 3b–3d). The improved shape can be traced in part to the nonzero A_0, since the surface contributes a larger fraction to the near-nadir than to the steeply viewing cameras, which flattens the reflectance difference curves. However, the 71°f and 60°f observed reflectances fall below the model when the lowest-residual MISR aerosol particle properties are used in the model.

[43] The particle physical properties derived by AERONET, MODIS, and MISR (mixture 11) are summarized in Tables 5 and 6. Size distributions and single-scattering phase functions are given in Figure 4 for the AERONET and MODIS particles and for MISR mixtures 11 and 63, both of which met the acceptance criteria used in the MISR Standard algorithm. Mixture 11 is 100% spherical, nonabsorbing particles, in a lognormal distribution having an effective radius of 0.12 microns and 1.7 micron characteristic width. Mixture 63 contains 40% of the 0.12 micron, nonabsorbing spheres, plus 48% medium mineral dust grain analogs, and 12% coarse mineral dust grain analogs. The SSAs for these mixtures are 1.0 and 0.98, respectively, but the Ångstrom exponents are 1.94 and 0.58; the AERONET-derived Ångstrom exponent was 2.01. This difference is also reflected in Figure 2b, where the shape of the spectral AOT curve for the MISR lowest-residual aerosol (mixture 11) matches that of the AERONET AOT extremely well, whereas the MISR best estimate spectral AOT curve, an average of all mixtures accepted by the algorithm, has a smaller slope. (The other two mixtures that met the acceptance criteria were very close to mixture 11, one having 80% of the 0.12 micron particle and 20% of the medium mineral dust grain analog, and the other having 100% of a particle with the same size distribution as that of mixture 11, but with midvisible SSA of 0.90 instead of 1.0.)

[44] The MODIS C4 particle sizes are closer to those retrieved by AERONET than the MISR particles (Figure 4a), but the fine/coarse ratio is higher for C5, giving an Ångstrom exponent (1.30) closer to that of AERONET and MISR than the C4 value (1.13). This is also reflected in the steeper slope of the MODIS C5 AOT curves compared to the C4 curves in Figure 2b. The larger components in MISR mixture 63 flatten the single-scattering phase functions in the 80° to 110° range (Figure 4b), producing closer agreement between the model and MISR observations for the 70°f and 60°f cameras in the green and red channels (Figures 3b and 3c). In reflectance units the difference is less than 0.009 in the green, 0.004 in the red, and 0.003 in the NIR, and could be due to a small residual fore and aft MISR camera calibration discrepancy such as that described in *Kahn et al.* [2005b]. Finally, in Figure 3 the wind and AOT adjustments do not produce any greater overall agreement than they did with the AERONET atmosphere.

[45] As illustrated by the analysis in this section, many factors must be well constrained to produce agreement at the level of detail considered here. The analysis also demonstrates the additional constraints on both aerosol and surface factors provided by the multiangle data. A summary of the conclusions reached regarding MISR-MODIS relative calibration, dark ocean water-leaving reflectance, and other surface boundary condition effects, particle-type assumptions, and algorithmic issues, is given in section 4. We return to the particle property discrepancy in section 3.3.

3.2. Ascension Island, 18 February 2005: Maritime Aerosol Gradients and Spatial Sampling

[46] Figure 5 examines a case where the Ascension Island AERONET reports much higher AOT values than nearby

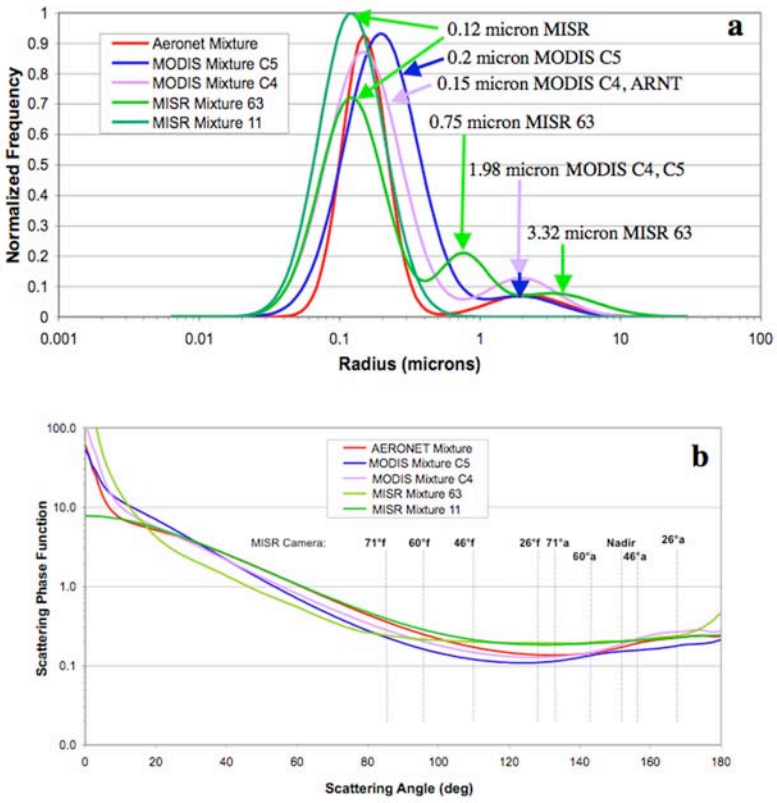

Figure 4. Retrieved particle properties for the 13 September 2003 Forth Crete event. (a) Area-weighted particle size distributions for AERONET fine and coarse-mode fits (red), MODIS C5 and C4 fine and coarse modes (blue and purple, respectively), and two of the lowest-residual mixtures retrieved by MISR (Table 5). Note that the MISR "best estimate" AOT is the average of the AOT retrieved for each mixture in the algorithm climatology that meets the acceptance criteria. In this case, four mixtures passed, two that are monomodal, r_{eff} = 0.12, with single-scattering albedo (SSA) = 1.0 ("mixture 11"; lowest residual) and SSA = 0.9, and two that are close to 50%–50% mixtures of the r_{eff} = 0.12, SSA = 1.0 particles and medium dust (mixtures 63 and 57). Mixtures 11 and 63 are plotted. (b) Green band scattering phase functions for the AERONET, MODIS, and two MISR aerosol mixtures identified in Figure 4a. The scattering angles sampled by the MISR cameras in this case are also indicated. (Note that the 26°f and 46°f cameras are in Sun glint, so only the 60°f and 71°f MISR cameras sample scattering angles smaller than 129°.)

MISR and MODIS values in a clean, primarily maritime aerosol air mass. On the basis of HYSPLIT back-trajectories (Draxler and Rolph, 2003) over the previous 5 days, moderate wind carried air NW over the south equatorial Atlantic. This air probably crossed the west coast of Angola or Namibia 6 or 7 days earlier and may have contained some biomass burning particles; the MODIS Fire Mapper (http://maps.geog.umd.edu/) does not indicate any significant fire activity in either country between 10 and 18 February 2005, though the FLAMBE aerosol web archive (http://www.nrlmry.navy.mil/flambe/index.html) reports considerable smoke over Zaire, Gabon, and Cameroon.

[47] Because such air masses are commonly assumed to have uniform aerosol loading when generating "Level 3" gridded aerosol products at coarse spatial resolution (e.g., 1° × 1°), available AOT data for any part of the scene is often assumed to represent AOT over the entire region. The example here illustrates some limitations of this assumption.

[48] Figure 5a shows that the MISR Standard algorithm retrieved AOT to the west of Ascension Island (green boxes). In the eastern potion of the image, MISR detected clouds, down to the smallest scale observed (275 m), and the MODIS C4 infrared water vapor retrieval [*Seemann et al.*, 2003] reported a jump in total column water vapor from about 3.5 to 4.5 precipitable centimeters along roughly the same boundary. Sun glint precluded MODIS aerosol retrievals (white boxes) closer than about 50 km west of the AERONET site. Three points having coincident MISR and MODIS AOT retrievals were selected for comparison with AERONET, as well as MISR retrieval region α, adjacent to the AERONET site, but without a coincident MODIS retrieval (Figure 5b). For this event we examine the apparent discrepancy between the satellite and Sun photometer AOTs.

[49] From Figure 5c, the AERONET AOT around Terra overpass time increased as air was advected from the east. AERONET retrievals also show an increase in atmospheric water vapor from 3.2 precipitable centimeters just before the overpass, to more than 3.4 cm a little more than an hour later. The lack of AERONET sky scan retrievals between 0935 UTC and overpass time may also indicate scattered cloudiness. So the AOT trend is likely a consequence of

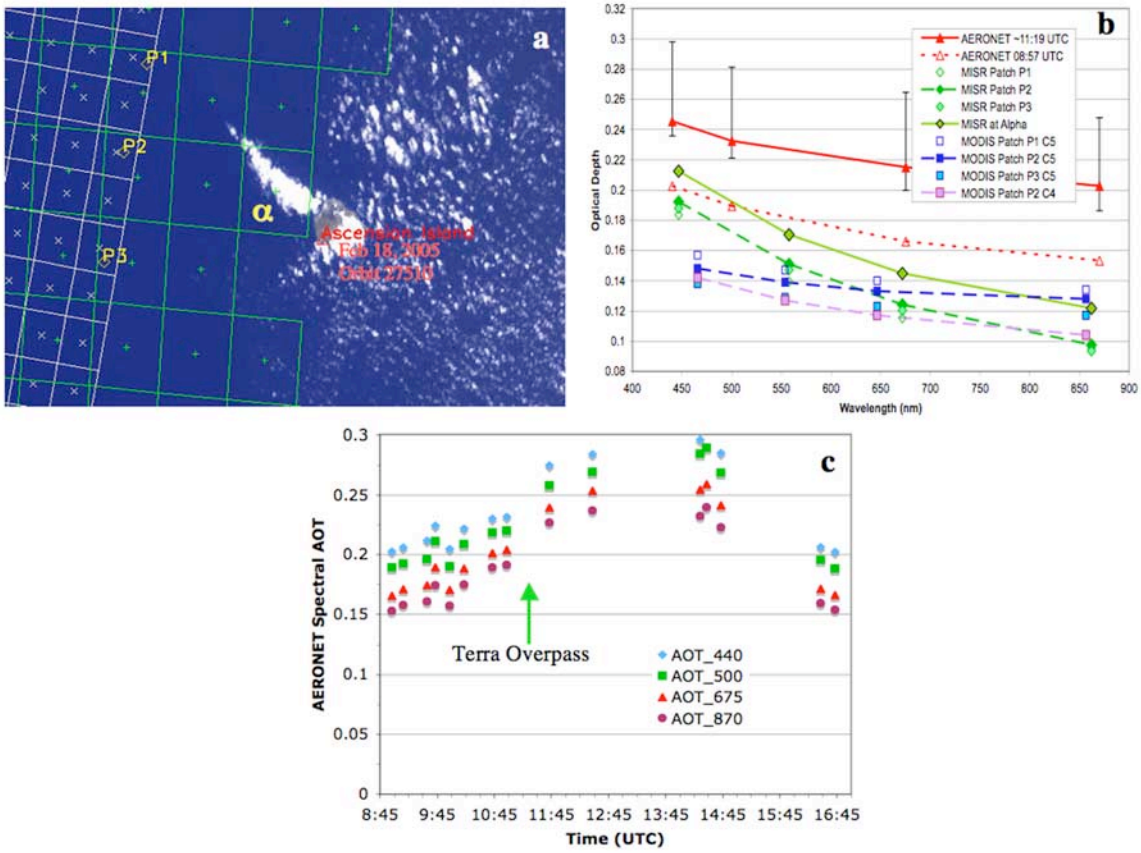

Figure 5. AOT analysis for the 18 February 2005 Ascension Island event. (a) Same as Figure 2a, but for Ascension Island and surrounding areas. (b) Best estimate MISR (green diamonds) and MODIS C5 (blue squares) Standard Aerosol product spectral AOT values plotted against band effective wavelength for retrieval regions containing patches P1, P2, and P3 (Figure 5a and Table 3) and the MISR retrieval at α, adjacent to the AERONET site. The MODIS C4 AOT values are given for P2 as well (purple squares). The AOT points for patch P2 are connected with dashed lines and for α they are connected with a solid line, to aid interpretation. Mean AERONET AOT values for three measurements taken 15 min apart around Terra overpass time are given as red triangles, connected by a solid line; whiskers represent the AOT range within approximately ±1 hour of overpass. In addition, the earliest available AERONET spectral AOT for that morning is plotted in open, red triangles. (c) AERONET spectral AOT time series around Terra overpass.

increased relative humidity, which can swell hygroscopic aerosols in the cloudier eastern air mass, although changes in aerosol amount or type, or subtle cloud contamination, cannot be ruled out as contributing factors.

[50] In Figure 5b the earliest available AERONET spectral AOT that morning is plotted as the red, dashed curve, highlighting the AOT increase during the 2.5 hours prior to the Terra overpass at that site. The range bars on the later AERONET curve in Figure 5b also reflect this AOT trend, for ±1 hour of the satellite overpass itself. No aerosol retrievals were performed by either MISR or MODIS on the eastern side of the MISR swath, where the air mass transition was observed. MISR retrievals closer to the AERONET site show a gradual increase in midvisible AOT to about 0.17 at patch α, but the jump to 0.23 and higher at the AERONET site and eastward, which appears to be a real change in AOT, was not captured by MISR or MODIS in this case. This result also illustrates that at least in some situations the current satellite aerosol retrieval algorithms preclude broken cloud regions.

[51] Using any one of these AOT products to represent an entire $1^\circ \times 1^\circ$ grid cell would likely produce sampling-related errors of order 0.1, on the basis of available data; MISR would report higher AOT than MODIS in part because it obtains results to the east, into the MODIS glint area, and AERONET would yield AOT higher still, because it samples just across the sharp transition to the moist air mass at Terra overpass time.

3.3. Ascension Island, 1 January 2005: Particle Properties

[52] The spectral slope of AOT is sensitive to particle size. MISR and MODIS coverage of Ascension Island on 1 January 2005, shown in Figure 6a, was very similar to that on 18 February (Figure 5), but in this case, nearby MISR midvisible AOT retrievals match well the AERONET values (Figure 6b). The MODIS C4 midvisible AOT is

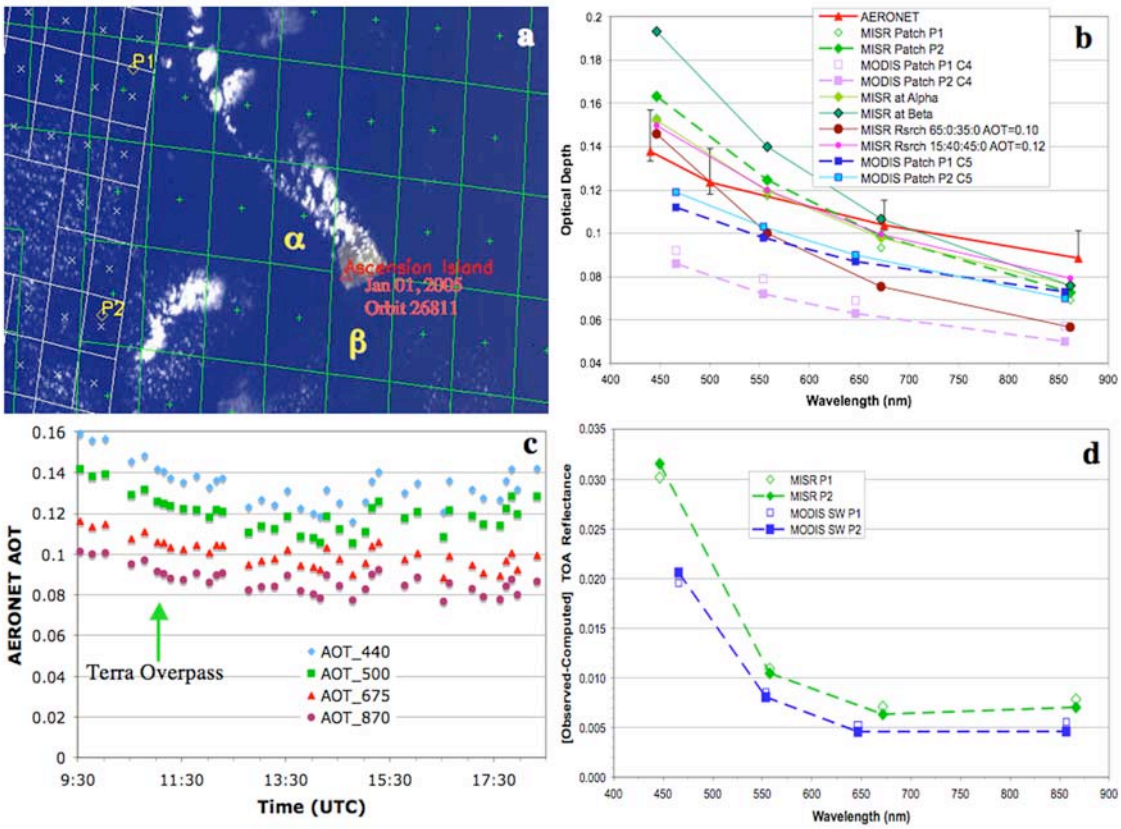

Figure 6. AOT analysis for the 1 January 2005 Ascension Island event. (a) Same as Figure 2a, but for Ascension Island and surrounding areas. (b) Best estimate MISR (green diamonds), MODIS C5 (blue squares), and MODIS C4 (purple squares) Standard Aerosol product spectral AOT values plotted against band effective wavelength for retrieval regions containing patches P1 and P2, and for MISR regions α and β (Figure 6a). The AOT points for patch P2 are connected with dashed lines, and for α and β they are connected with thin solid lines, to aid interpretation. Mean AERONET AOT values for three measurements taken 15 min apart around Terra overpass time are given as red triangles, connected by a solid line; whiskers represent the AOT range within approximately ±1 hour of overpass. Also shown are the spectral AOT curves for two MISR Research Retrieval results, each designated by the percent midvisible AOT of standard MODIS components: 1 (r_e = 0.1 microns), 2 (r_e = 0.15), 6_C5 (r_e = 1.48), and 7_C4 (r_e = 1.98) (see Table 6 and text for details). (c) AERONET spectral AOT time series around Terra overpass. (d) Same as Figure 2d, but for Ascension study patches P1 and P2.

about 0.04–0.06 lower than AERONET, whereas for MODIS C5 it is only about 0.02 lower. As on 18 February, the AOT spectral slopes for both MODIS versions match that of the AERONET measurements, whereas the MISR slope is steeper. Again, on the basis of HYSPLIT back trajectories (Draxler and Rolph, 2003) the air at all levels spent the previous week or more traveling east over the South Atlantic at average wind speeds below 7 m/s. In this case the lower-level air may have crossed the Namibian coast prior to that, whereas the air at 3 km appears to have come from the Cameroon and Gabon region farther north.

3.3.1. Midvisible AOT Differences

[53] Unlike the 18 February case, the AOT does not exhibit a strong aerosol air mass boundary or other scene variability between the AERONET site and the MODIS-MISR coincident aerosol retrieval region to the west. This is demonstrated by the similarity in MISR green, red, and NIR AOT results at P1, P2, and α (Figure 6b) and by the relatively flat AERONET AOT time series over much of the day (Figure 6c). The MISR Standard Retrieval for patch β has a steeper slope, which may be due to a subtlety in the V17 algorithm that causes it to perform a difficult overland retrieval with only a few island pixels in a mostly water region. (This is discussed further in section 3.4, with regard to regions α and β in Figure 9a.) In this case the 6 m/s near-surface wind speed assumed in the MODIS algorithm is within measurement uncertainty of the observed speed, so this is unlikely to contribute significantly to the low MODIS-retrieved AOT. More generally, if there were any errors in the retrieval algorithm surface model or cloud screening, the likely corrections would further decrease the MODIS-derived AOT relative to AERONET. So aerosol horizontal variability and the surface model assumed by the retrieval algorithm seem unlikely to account for the low AOT retrieved by MODIS.

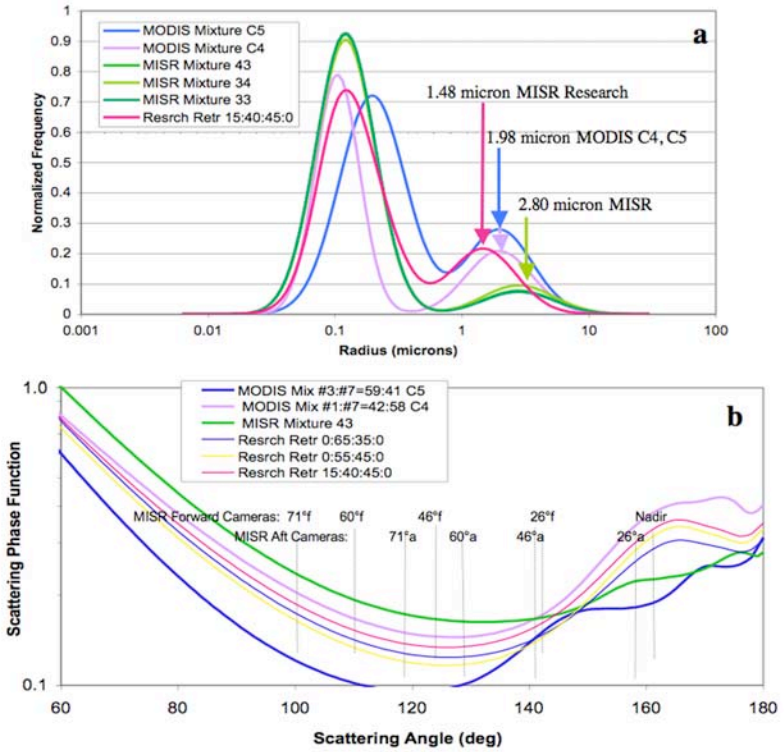

Figure 7. Retrieved particle properties for the 1 January 2005 Ascension Island event. (a) Area-weighted particle size distributions for MODIS C5 and C4 fine and coarse modes (blue and purple, respectively), the three lowest-residual mixtures retrieved by the MISR Standard algorithm, and the 15–40–45–0% result from the MISR Research retrieval. (b) Green band scattering phase functions for the MODIS, AERONET, one MISR standard, and three MISR Research Aerosol mixtures. The scattering angles sampled by the MISR cameras in this case are also indicated. (Note that the 26°f and 46°f cameras are in Sun glint, so only the 60°f and 71°f MISR cameras sample scattering angles smaller than 129°. Also, the MODIS mixtures in the figure legend are given as percents of MODIS component models listed in Table 6.)

[54] Figure 6d shows the TOA reflectance differences between MISR and MODIS at patches P1 and P2, relative to the forward radiative transfer model, run with the AERONET-derived atmosphere, the observed wind speed, and the A_0 values used in the standard algorithms. Differences between the MODIS and model reflectance values are about +0.005 and +0.008 in the red and green bands, about twice the corresponding values for patches P2 and P3 of the Forth Crete event (Figure 2d), though the midvisible AOT is similar for the two events (Figures 2b and 6b). Compared to the nominal model, the MISR-MODIS reflectance differences remain proportionately about the same as for Forth Crete. So the MODIS reflectances do not appear to be unduly low, as might occur if the reflectance histogram truncation used in the MODIS processing had skewed the values.

[55] For both MODIS and MISR the aerosol type adopted by the algorithm also affects retrieved AOT. The midvisible SSA used in the MODIS retrieval for this event is 0.92 for Collection 4 and 0.98 for Collection 5, whereas the corresponding MISR value is 0.84 (Table 4). However, this was a clean, maritime air mass that had been over the Atlantic for more than 5 days, and even the source areas in Africa did not have any reported fires when the air was over land, so SSA values lower than 0.9 are suspect. (The AERONET quality statement indicates that retrieved SSA should be used only when AOT > 0.4 [*Dubovik et al.* 2000]; for this case, AOT < 0.2.) So the best available data suggest that the AERONET AOT, determined from direct Sun measurements independent of any aerosol model, must be matched with particles having midvisible SSA > 0.9. Compared to the 0.12 AOT retrieved by MISR, the lower AOT retrieved by both versions of the MODIS algorithm, 0.08 and 0.10 for C4 and C5, respectively, is partially explained by the less absorbing (brighter) particles adopted in the MODIS retrievals.

[56] All other things being equal, if the particles are assumed brighter, a lower AOT is needed to match the observed TOA reflectance. However, the change from MODIS Collection 4 to Collection 5 produces an increase in SSA for the best-fitting model from 0.92 to 0.98 and an increase in AOT from 0.08 to 0.10. This pattern is traced to changes in the particle single-scattering phase function for the nadir viewing geometry, which falls near 160° scattering angle (Figure 7b). Although the SSA and AOT both increased for the particles selected by the Collection 5 algorithm, the fraction of light scattered into the near-nadir direction observed by MODIS is reduced by about a factor

of 2 because of the change in phase function at these angles. This requires a compensating increase in AOT relative to that obtained in Collection 4, as observed in Figure 6b.

3.3.2. AOT Spectral Slope Differences

[57] Despite the midvisible AOT agreement between MISR and AERONET, the MISR-retrieved AOT spectral slope is steeper than that derived from direct Sun AERONET measurements (Figure 6b). Particle size distributions favoring smaller particles can produce steeper spectral AOT slopes, though the bimodal nature of the particle mixture must be taken into account in the analysis. Figure 7a shows the area-weighted size distributions for the retrieved MODIS C4 and C5, the three lowest-residual MISR Standard algorithm aerosol mixtures, and the lowest-residual MISR Research Retrieval mixture. The MISR research retrieval mixture is composed of the following components: 15% midvisible AOT of MODIS Model 1 (r_e = 0.1 microns, small), 40% of MODIS Model 2 (r_e = 0.15, medium, having both larger r_e and larger distribution width than the 0.1 micron particles), 45% of MODIS Model 6_C5 (r_e = 1.48), and 0% of MODIS Model 7_C4 (r_e = 1.98) (designated 15:40:45:0; see Tables 5 and 6). All retrievals shown here except the C5 MODIS have a medium-mode particle with effective radius around 0.1 microns, but the coarse-mode sizes are distinctly different; the MODIS distributions for both C4 and C5 peak at 1.98 microns, whereas MISR has a smaller peak at 2.8 microns. Here the MODIS solution is consistent with the best available data, since the resulting spectral AOT slope matches that of AERONET (Figure 6b), and the AERONET slope comes from direct Sun measurements, independent of any particular two-component aerosol model. (Interesting, though as yet unexplained, is the observation that the MODIS C4 and C5 retrievals, which selected different SSAs, AOTs, fine-mode particle sizes, and fine/coarse ratios, produced nearly the same Ångstrom exponents (Figure 6b).)

[58] The V17 MISR Standard Aerosol Retrieval algorithm does not contain coarse-mode particles having effective radii between 1.0 and 2.8. So a modest amount of the 2.8 micron particles was chosen by the standard algorithm to match the observed reflectances. Because the single-scattering phase function for the 2.8 micron particle has a distinctly different shape from the smaller coarse-mode particles (Figure 7b), to match the phase function behavior, the algorithm combined this with a larger AOT fraction of medium-mode particles, producing too steep a spectral AOT slope. The MISR Research Retrieval algorithm allows us to explore this situation further.

[59] Figure 8a illustrates how the MISR Standard V17 lowest-residual aerosol mixture, the MODIS Standard Collection 4 best fit aerosol mixture (42% MODIS Model 1, 58% MODIS Model 7_C4), the MODIS Standard Collection 5 best fit aerosol mixture (59% MODIS Model 3, 41% MODIS Model 7_C4), and three MISR Research Retrieval mixtures each fit the range of MODIS TOA spectral reflectance observations at patch P1. The three Research Retrieval mixtures selected represent the lowest-residual Research Retrieval mixture (designated 15:40:45:0 using the notation described above), a mixture for which the smallest component's AOT contribution is added to the medium (r_e = 0.15) component (0:55:45:0), and one having a higher small-component AOT fraction, similar to that retrieved by the MISR Standard V17 algorithm, but using the same components as the other two Research Retrieval mixtures (65:0:35:0). As expected, in all cases the shortest-wavelength channels do not fit the observations well, since the standard A_0 values are assumed in the model. At the longer wavelengths the performance of all the nadir models is within 0.004 of the MODIS observations.

[60] Figures 8b through 8d show multiangle performance at three wavelengths, so model comparisons can be made against MISR observations only. The green band AOT is set to 0.143 for the MISR Standard lowest residual and 0.118 for the MISR Research and MODIS Standard best fit cases, except the 65:0:35:0 AOT = 0.10 case. The peaks for the 26°f and nadir cameras, which become more pronounced at the longer wavelengths, indicate that the observations are relatively brighter than the model for these cameras. This could well be due to unscreened glint; the glint angle for these two cameras is about 42° and 41°, respectively, just past the arbitrary 40° cutoff of the glint mask. The moderate wind speed on this day (Table 1) suggests angular spreading of the glint pattern is likely [e.g., *Fox et al.*, 2007], and the increased size of the effect for longer wavelengths and near-nadir cameras probably indicates increased sensitivity to surface properties for these channels.

[61] The MISR Research Retrieval mixtures containing fractions of the 1.98 or 1.48 micron coarse-mode particles similar to those retrieved by MODIS C4 (Table 5), but with the higher AOT obtained by the MISR Research Retrieval, reproduce the observed angular behavior better than the lowest-residual option available in the MISR V17 Standard algorithm, especially in the red and NIR bands used for the MISR overwater retrieval. Although differences among most of the cases shown are slight, the 15:40:45:0 mixture has the lowest residual in the Research Retrieval run; this shows up most in the 46°, 60°, and 71° fore and aft cameras, which are most sensitive to the aerosols.

[62] When the fraction of small particles is increased, a larger proportion of light is scattered into the sideward directions observed by MISR, so the model AOT must be reduced to match the observed brightness. As shown in Figure 8b–8d for the 65:0:35:0 mixture, an AOT reduction of 0.02 brings this model into the range of the others. The MISR Standard lowest-residual mixture, having a larger fine/coarse particle AOT ratio, provides the poorest angular spectral fit to the observations in the red and NIR bands used in MISR overwater retrievals. Returning to Figure 6b, the Research Retrieval spectral optical depths for the 15:40:45:0 mixture, which contains a greater fraction of larger aerosol components, provides a better match to the AERONET spectral AOT slope, whereas the 65:0:35:0 case, having a larger fraction of smaller particles, produces too steep a slope, closer to the Standard algorithm result.

3.4. Tahiti, 12 August 2001: Broken Cloud and Uniform Brightening

[63] Figure 9a shows a broken cloud scene. As in Figures 2a, 5a, and 6a, green and white boxes indicate where MISR and MODIS Standard Aerosol Retrievals were performed, respectively. Constraining the sea state is difficult in this case. The surface wind measured at Tahiti's Faa'a International Airport was very low for this event (Table 1); that site appears to be in the lee of the island. The SeaWinds instrument on the QuikSCAT satellite retrieved

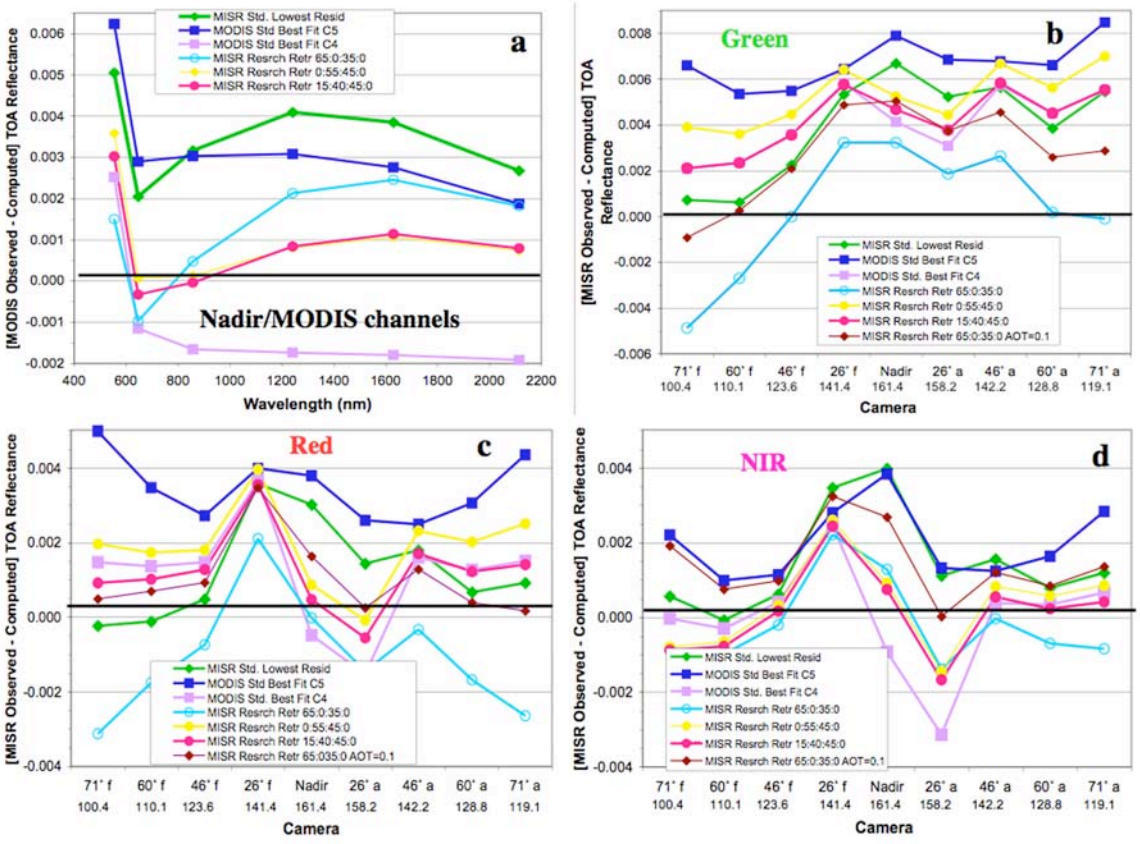

Figure 8. Multiangle reflectance analysis for the 1 January 2005 Ascension Island event. (a) (MODIS observed – modeled) nadir-viewing spectral TOA equivalent reflectance differences for models run with the MISR Standard V17 retrieved lowest-residual atmosphere, the MODIS Standard C5 and C4 best fit aerosol mixtures (with midvisible AOT set to the AERONET value of 0.118), and three MISR Research Retrieval atmospheres with midvisible AOT set to 0.118; (b) green band (MISR observed – modeled) TOA reflectance differences for the same atmospheres used for Figure 8a, plus the 65:0:35:0 model with midvisible AOT reduced from 0.118 to 0.10, showing all MISR cameras. The scattering angles for each camera are given below the camera names in the horizontal axis label. (c) Same as Figure 8b, but for red band. (d) Same as Figure 8b, but for the near-infrared (NIR) band.

surface wind speeds on order of 13 to 15 m/s in the open ocean, with lower wind speeds near Tahiti itself (http://podaac.jpl.nasa.gov). This difference complicates the interpretation of the MISR and MODIS observations.

[64] Consistent with the QuikSCAT wind direction, the lower-level air came from the South Pacific, moving NW, and the upper level air came from the Pacific to the east, on the basis of HYSPLIT back-trajectories (Draxler and Rolph, 2003). This maritime air mass had a midvisible AOT of 0.064, as measured by AERONET, about 3 times lower than the values retrieved by MISR and MODIS at three patches as little as 20 km away (P1, P2, and P3, and Figure 9a); both algorithms assessed these locations as sufficiently cloud-free and glint-free to report results (Figure 9b). Until about 2100 UTC, 40 min after the Terra overpass, the AERONET station did not report AOT values, most likely because of cloud interference.

[65] Figure 9c, a stretched version of the MISR nadir view that includes the AERONET site and surrounding satellite retrieval region, reveals a subtle increase in brightness near the Tahiti site (light purple), over the area that appears cloud-free in Figure 9a, and two smaller areas in the lee of the island that do not exhibit this brightening (darker blue in Figure 9c). The brightening could be a thin, near-surface atmospheric haze, or a subtle, water or air flow-driven change in ocean surface reflectance in the island's wake. The feature has a sharp boundary that does not show parallax in the multiangle views, suggesting a surface or near-surface phenomenon. In addition, the contrast across the boundary over the forward viewing cameras does not change, which could be caused by haze or uniform surface reflection. In either case the enhanced TOA brightness passed both MISR and MODIS cloud and glint screening algorithms. However, it also increased the satellite-retrieved midvisible AOT by approximately 0.1, on the basis of the difference between the satellite AOT values and AERONET direct Sun measurements. Uniform brightening of this sort occurs frequently in cases of broken cloud over the ocean.

[66] To further explore retrieval behavior in regions containing significant fractions of broken cloud cover, satellite-derived, midvisible AOT along two traverses (red diamonds in Figure 9a) are plotted in Figures 9d and 9e. Trace 1 runs

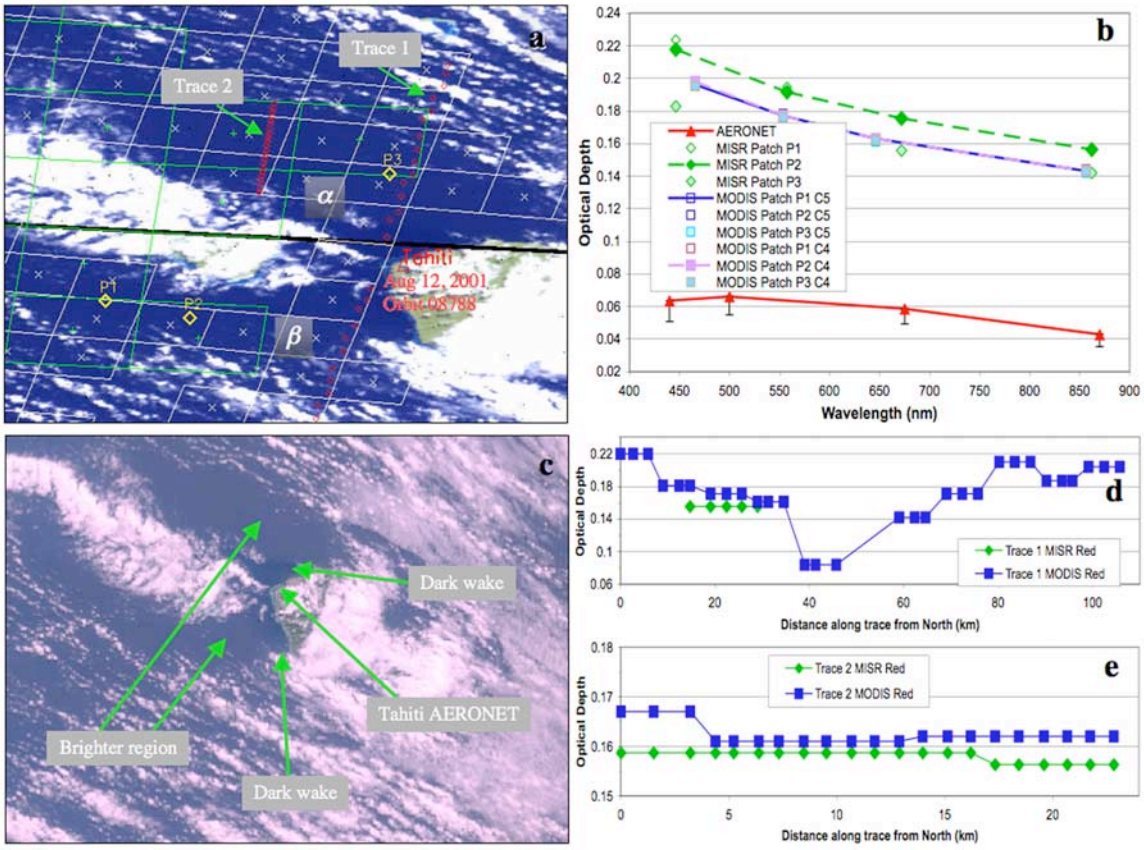

Figure 9. AOT retrieval analysis for a broken cloud scene, Tahiti, 12 August 2001. (a) Same as Figure 2a, but for Tahiti and surrounding areas. The traverses plotted in Figures 9d and 9e are mapped as red diamonds here. (b) Best estimate MISR (green diamonds) and MODIS C5 and C4 (blue and purple squares, respectively) Standard Aerosol product spectral AOT values plotted against band effective wavelength for retrieval regions containing the three patches (Table 3). The AOT points for patch P2 are connected with dashed lines to aid interpretation. Mean AERONET AOT values for three measurements taken 15 min apart, starting about 40 min after Terra overpass, are given as red triangles, connected by a solid line; whiskers represent the AOT range over the AERONET measurement period. (c) Stretched version of the MISR nadir red-green-blue image. Thin haze to the west and north of the Tahiti site appears in light purple. (d) MISR and MODIS C5-retrieved red band aerosol optical depth along trace 1 in Figure 9a. (e) MISR and MODIS C5-retrieved red band aerosol optical depth along trace 2 in Figure 9a.

NNE to SSW across 10 MODIS Retrieval regions close to the Tahiti AERONET site and passes through one MISR Retrieval region. The MODIS AOT (blue squares) agrees well with the MISR values (green diamonds) between 15 and 30 km along the trace, where they coincide. The MODIS values diminish to about 0.08 between 40 and 50 km along the trace. Here MODIS is coincident with the AERONET site, the retrieval region includes the dark island wake (Figure 9c), and the AOT results are in very good agreement. So in this case, surface reflectance spatial variability seems to be a key factor affecting the retrieved AOT values (Figure 9b); it must be taken into account when aggregating to coarser resolution Level 3 products.

[67] The MISR Standard algorithm did not report aerosol retrievals in regions α and β in Figure 9a, despite many 1.1 km pixels in each region that are apparently cloud free. This is traced to a subtlety in the Standard algorithm logic (V17 and earlier). If a region contains any land pixels (as determined by the static land/ocean mask), the algorithm attempts an overland retrieval using only the land pixels. This approach works well over major coastal areas, where the near-coastal water surface is likely to be brighter than assumed in the overwater algorithm. However, near-isolated, deep ocean islands, a retrieval region may contain only a few land pixels, and if these are cloud contaminated or topographically complex, for example, no aerosol retrieval will be done.

[68] Trace 2 of this complex scene runs through the uniform, brighter region farther west, covering two MISR and three MODIS retrieval cells (Figure 9a). Figure 9e gives the standard AOT retrieval results: MODIS C5 and MISR red band AOT are within 0.01 over most of the coincident path, though MODIS tends to be higher despite having absolute calibration lower than MISR, and an assumed wind speed higher than that adopted by MISR, both of which would lower the MODIS-retrieved value. In this case the difference in radiance selection strategies seems to be

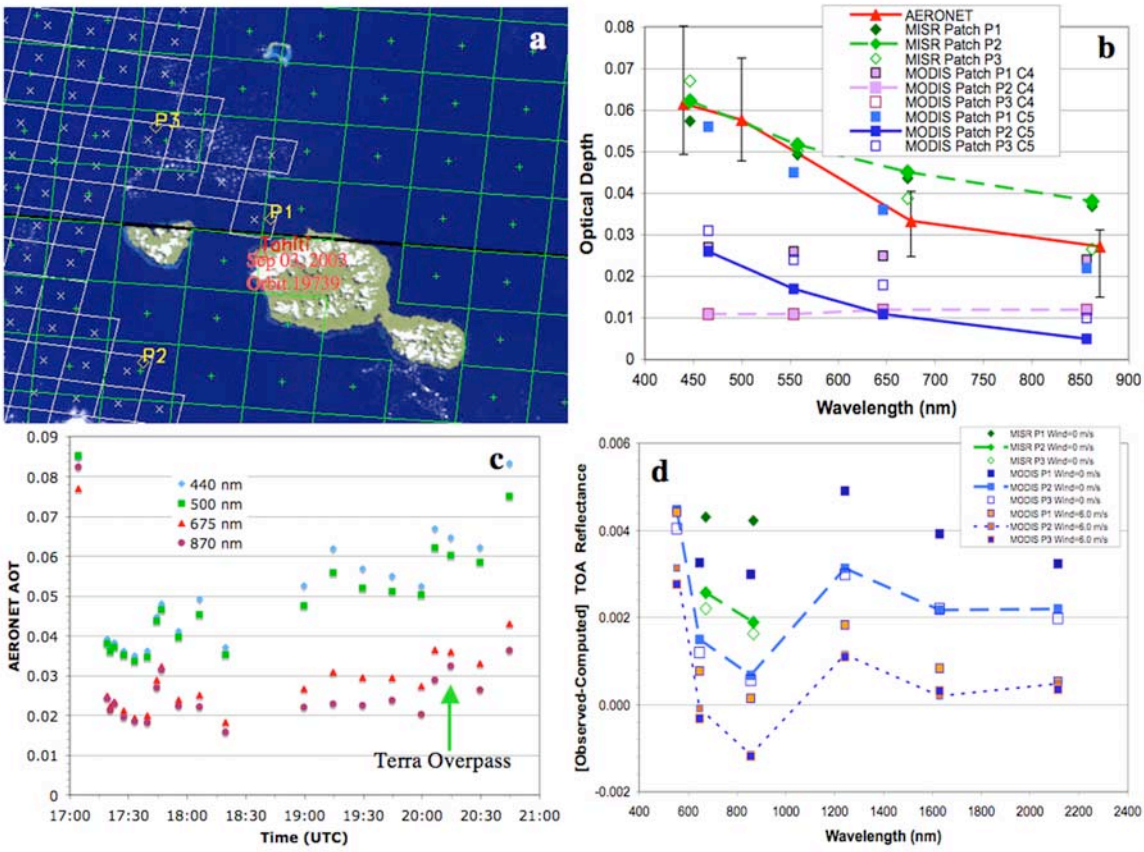

Figure 10. AOT analysis for the 3 September 2003 Tahiti event. (a) Same as Figure 2a, but for Tahiti and surrounding areas. (b) Best estimate MISR (green diamonds) and MODIS C5 and C4 (blue and purple squares, respectively) Standard Aerosol product spectral AOT values plotted against band effective wavelength for retrieval regions containing patches P1, P2, and P3 (Figure 10a and Table 3). The AOT points for patch P2 are connected with dashed lines to aid interpretation. Mean AERONET AOT values for three measurements taken 15 min apart around Terra overpass time are given as red triangles, connected by a solid line; whiskers represent the AOT range within approximately ±1 hour of overpass. (c) AERONET spectral AOT time series around Terra overpass. (d) Differences between MISR nadir or MODIS observed TOA reflectances and model values for three patches in three MISR and six MODIS spectral bands, each evaluated and plotted at the effective wavelength of the observation. The model assumes the AERONET-derived AOT and particle properties for this event (Table 4), the observed surface pressure and wind speed (Table 1), and as in the Standard Satellite Retrieval algorithms, $A_0 = 0$ except for the MODIS green band, where it is 0.005. In addition to simulations based on the observed wind speed, MODIS channel simulations are given for 6 m/s, as assumed in the MODIS Standard algorithm. The patch P2 MISR and MODIS points are connected with straight lines to aid interpretation.

responsible. The MISR algorithm selects the darkest pixel in the retrieval region, whereas the MODIS algorithm truncates the lowest 25% of the reflectance histogram, which is effective in eliminating cloud shadows, but not in cases where only a small fraction of the pixels are not contaminated with uniform haze. Each approach has advantages in some situations; an automatic algorithm for determining when each should be used would probably need to assess scene spatial heterogeneity in a way that has yet to be developed.

3.5. Tahiti, 3 September 2003: Low Near-Surface Wind

[69] Near-surface winds were from the east at Tahiti, at about 1.4 m/s, and HYSPLIT back-trajectories (Draxler and Rolph, 2003) showed that upper level winds had circled from the east over the previous 5 days, arriving from the NW on 3 September 2003. The air mass was maritime, and the midvisible AOT about 0.05 (Tables 1 and 4). The scene had a few scattered clouds (Figure 10a), MISR aerosol retrievals were obtained over the entire region, whereas MODIS performed retrievals mostly to the west of Tahiti, in the area that was glint-free at nadir.

[70] Despite the apparent simplicity of this scene, Figure 10b shows some disagreement among the retrieved MISR, MODIS, and AERONET spectral AOTs. For patches P2 and P3, midvisible AOT for MISR and AERONET concur to within 0.01 at all wavelengths, whereas the MODIS C4 and C5 AOTs for both sites are about 0.05 smaller. For patch P1, very near the AERONET site, MODIS C4 falls about 0.025 below the other results,

whereas the C5 spectral AOT is in agreement with AERONET. The AERONET time series (Figure 10c) shows an AOT increase of about 0.02 during the 3 hours prior to Terra overpass, and the MISR regional snapshot does not exhibit any apparent gradients, all suggesting that the AOT at the MODIS patches should be close to the AERONET values.

[71] One contributor to the low MODIS AOT values is the 6 m/s surface wind speed assumed by the MODIS algorithm. The observed wind speed was 1.4 m/s in this case (Table 1), and the MISR climatology reported a value of 2 m/s. Figure 10d shows the difference between the MODIS observed TOA spectral reflectances and those calculated with the forward radiative transfer model, assuming surface wind speeds of 0 and 6 m/s. The high wind speed assumed by the MODIS algorithm drives the retrieved midvisible AOT down by about 0.02, which can account quantitatively for more than half the MODIS AOT deficit in the green, and all of it at longer wavelengths. In this low-AOT, low-wind case the unduly high, assumed wind speed apparently removes most of the signal that the MODIS algorithm would otherwise attribute to aerosols.

[72] Particle properties also play some role, as demonstrated by differences as large as 0.03 between the C4 and C5 AOT. The spectral slope of the MODIS C4 AOT is much flatter than for MISR and AERONET in this case. Table 5 indicates that AERONET retrieved 73% fine-mode and 27% coarse-mode particles, MISR obtained 40% fine, 36% medium, and 24% coarse, whereas MODIS C4 derived only 24% fine, and 76% coarse. However, MODIS C5 retrieved 100% fine-mode particles for each of the three patches, though the MODIS C5 algorithm retrieved different sized fine-mode particles in each. This does explain the slope differences in Figure 10b, but it also illustrates further the difficulty in extracting particle property information from TOA radiances when the AOT is below about 0.1, even over a dark, uniform surface [e.g., *Kahn et al.*, 2001a].

4. Discussion and Conclusions

[73] We set out to understand systematic differences that occur among the current MISR (V17), MODIS (Collections 4 and 5), and AERONET (V2, Level 2 for direct Sun and primarily Level 1.5 for sky scan) retrieved aerosol optical thickness products. Accordingly, we analyzed in detail five MISR-MODIS-AERONET coincident events over dark water sites, representing the common AOT discrepancy patterns we found in an extensive search of the data sets. These are all relatively low optical depth events (midvisible AOT < 0.23), as is typical over ocean away from coastal regions and major dust or smoke clouds. We conclude the following:

[74] 1. Even for dark water cases where there are midvisible AOT discrepancies among the current standard retrieval algorithms, the results generally fall within the previously reported uncertainties of order 0.05. This represents a major step beyond what was possible with the previous generation of spaceborne, Earth-observing instruments, opening a range of new global and regional aerosol applications for satellite data.

[75] 2. However, applications requiring AOT accuracies of 0.03 or better demand further algorithm refinement, to the extent possible. We identified several systematic discrepancy patterns, and traced them to instrument calibration and sampling differences, to assumptions made in the MISR and MODIS Standard Aerosol Retrieval algorithms about ocean surface boundary conditions, missing particle property or mixture options, and the way reflectances used in the retrievals are selected. Cloud screening is also a factor, skewing the satellite results higher than the actual AOT in some situations; this issue is the subject of separate studies.

[76] 3. As discussed in previous work, the absolute calibration scale for MISR is higher than MODIS by about 3% in midvisible because of differences in the standards used to set these scales. Other factors such as the surface boundary condition and aerosol model being equal, this can produce retrieved midvisible AOT differences on order 0.01–0.02 for typical dark ocean situations. This difference could be resolved by a study comparing statistically significant samples of several retrieved geophysical quantities, such as AOT and surface albedo, with ground truth and determining if the results are skewed in the same sense for one instrument or the other.

[77] 4. Natural ocean surface midvisible water-leaving reflectance commonly varies by factors of 2 or 3 on 10 km scales, especially near coasts. The current MISR and MODIS Standard algorithms assume the spectral water-leaving reflectance (A_0) is zero except in the MODIS green band, where A_0 is set to 0.005. Actual dark water A_0 values are typically 0.007, 0.002, and 0.0007 in the green, red, and NIR, respectively. (The blue TOA reflectance is so dominated by the assumed A_0 value in typical ocean cases that this band is not used over ocean in either the MISR or MODIS Standard Aerosol Retrieval algorithms; for the same reason the current MISR algorithm avoids the green channel as well.) The low assumed A_0 values can bias the satellite-retrieved midvisible AOT high by about 0.01 to 0.02 over dark water and can create artificial variability in retrieved AOT of greater magnitude where the surface water is infused with silt, pollution, phytoplankton, or other reflecting material. For the example in section 3.1, an increase in water-leaving reflectance of about 0.005 to 0.008 in all bands is the likely cause of ~0.04 MISR- and MODIS-retrieved midvisible AOT increases, relative to otherwise imperceptibly darker water nearby. Errors in the assumed spectral A_0 values can also affect the reflectance spectral slopes used for the aerosol retrieval, which in turn will influence derived aerosol properties. It may be possible to derive A_0 from the MISR multiangle data, provided the aerosol properties and near-surface wind speed can also be well constrained.

[78] 5. In many cases the MODIS Standard algorithm's assumed ocean surface wind speed of 6 m/s everywhere compensates for low assumed A_0, whereas MISR uses a monthly, global wind speed climatology that produces generally lower ocean surface reflectance compared to MODIS. Using a statistical approach, *Zhang and Reid* [2006] reached a similar conclusion. These factors leave the MISR-retrieved AOTs biased high when A_0 is larger than zero and skew MODIS values low when the ocean surface is both dark and calm. In large statistical summaries, MISR midvisible AOT over water is typically 0.02 to 0.03 higher than MODIS, most likely because of the combination of calibration and assumed wind speed differences. The MODIS wind speed assumption can eliminate sensitivity to AOT at least as high as 0.04 in midvisible wavelengths,

under dark, calm conditions. More generally, for the nadir-viewing MODIS instrument the wind-speed-related surface assumption may dominate the aerosol retrieval result when the AOT is low, especially at the longer wavelengths, where AOT is generally even lower than in the visible. Wind speeds derived adaptively, e.g., from the angular width of the glint pattern [*Bréon and Henriot*, 2006; *Fox et al.*, 2007], from other satellite instruments, or from global weather models, can reduce or eliminate this source of AOT retrieval error.

[79] 6. Differences in aerosol type adopted by the MISR and MODIS Standard algorithms as part of the retrieval process can also translate into AOT differences. Specific aerosol components and mixtures are available in the Standard algorithms, and these options must be rich enough to cover the range of commonly occurring aerosol types, with gradations appropriate to instrument sensitivity [e.g., *Kahn et al.*, 2001a, 1998]. In several cases studied here the lack of a spherical particle having effective radius between 1.5 and 2 microns in the MISR Standard algorithm produced unduly steep spectral AOT slopes. Systematic examinations of MISR sensitivity to mineral dust [*Kalashnikova and Kahn*, 2006] and smoke particles (W.-T. Chen et al., Sensitivity of multi-angle imaging to optical and microphysical properties of biomass burning particles, submitted to *Journal of Geophysical Research*, 2007) have recently been completed. Work continues on these and other particle types, taking advantage of coincident, height-resolved aerosol and surface property measurements made during the UAE-2, INTEX-A and B, SAMUM, and GoMACCS field campaigns. Parallel conclusions about the MODIS standard algorithm's sensitivity to particle type assumptions were reached by *Zhang and Reid* [2006].

[80] 7. Differences in the particle characteristics assumed by the Collection 4 and Collection 5 MODIS aerosol retrieval algorithms affected the retrieved AOTs and fine/coarse ratios, even over dark water. The contributions of these assumptions to the systematic differences among satellite and surface AOT products are among the factors being evaluated by the MISR and MODIS teams as part of continuing work.

[81] 8. Choices about the way reflectances are selected by the algorithms produce biases under some circumstances. For example, if unscreened clouds occur in the retrieval region, the MODIS Standard algorithm approach of eliminating the top and bottom 25% of the reflectance histogram can produce anomalously high AOT retrievals. If unscreened clouds such as thin cirrus contaminate an entire retrieval region, the MISR Standard algorithm approach of selecting the darkest pixels will produce anomalously high AOT retrievals as well. Conversely, if cloud shadows are present, the MISR algorithm can produce anomalously low AOT values. Automatic procedures for identifying such circumstances in the satellite imaging data have yet to be developed.

[82] 9. Spatial sampling differences produce apparent discrepancies among MISR, MODIS, and AERONET when the instruments capture real aerosol gradients or different aerosol air masses. Even for clean maritime conditions, midvisible AOT can change by 0.1 or more over the tens of kilometers that may separate instrument retrieval regions. If not recognized, major dust or smoke clouds observed by one instrument but not another can skew "Level 3" gridded, space- and time-averaged products.

[83] The issues identified in this study produce discrepancies that are insignificant at many sites and for many applications. However, most are not random, so they bias the results when large numbers of satellite AOT measurements are aggregated, such as in large-spatial-scale and long-time-series climatological analyses of aerosol direct radiative forcing or net aerosol transport estimates. The commonly made assumption that measurement error diminishes as the square root of the number of measurements aggregated does not apply to systematic biases. Midvisible AOT errors of order 0.02 to 0.03, amounting to a few Wm^{-2} in radiative forcing for typical maritime situations, can be expected unless these effects are removed from the data sets.

[84] If current algorithm limitations will affect the results of a study, many of them can be avoided by working with the orbit-by-orbit (Level 2) satellite aerosol products. When aggregated Level 3 products are used, several considerations can limit the impact of systematic overwater AOT biases:

[85] 1. Take sampling into account, as appropriate. When there are few samples in an aggregate, a single, optically thick event can dramatically skew the average. Simply tracking the number of counts per space-time sampling bin (N) goes a long way toward identifying this possibility. N is included in the standard MISR and MODIS Level 3 products, so subsets of these products can be created on the basis of the minimum number of observations needed in each bin for a particular application. One should at least look at some measure of spread, such as the standard deviation of the quantity of interest, especially if N is small.

[86] 2. Bear in mind that despite the handful of coincident cases identified for the current study, MISR and MODIS Terra sampling are quite different, and their retrieval areas over water frequently do not overlap, since MODIS is in Sun glint over the narrower MISR swath much of the time, whereas MISR relies on the off-nadir cameras for aerosol retrievals where the nadir view is glint contaminated. MISR observes the entire Earth about once per week, whereas MODIS sees it about once in 2 days; cloud contamination eliminates many observations, preferentially in cloud-prone regions. On a global, monthly basis, short-lived, severe aerosol events such as dust storms and wildfires dominate averaged aerosol quantities in some seasons and locations. Given the sampling differences, these events may be observed by one but not the other instrument; in this regard the two data sets may be complementary.

[87] To make the most reasonable use of these two complementary satellite data sets, the following approaches are recommended:

[88] 1. If possible, aim for targeted regional rather than naive global analyses. Try to avoid times and places where the standard algorithm ocean surface model assumptions are likely to be inaccurate, such as situations where runoff, major phytoplankton blooms, or shallow water may produce high water-leaving reflectances or where near-surface wind speeds are generally different from those assumed by the algorithms. The current automatic algorithms eliminate some but not all such cases. Also, building on the approach of this paper, differences in the MISR and MODIS Standard

product AOT values may be used to identify situations that violate algorithm assumptions.

[89] 2. Use consistent, validated versions of the products. It takes about 3 months to reprocess a year of MISR data with a new version of the algorithm, and currently available Levels 2 and 3 products covering periods of a year or more may include a mix of validated and unvalidated versions.

[90] 3. Take seriously the product quality statements, which describe cloud-screening limitations and validation sensitivity study results.

[91] The satellite instrument teams are further upgrading the aerosol retrieval algorithms. For example, work is currently underway aimed at reducing or possibly eliminating the MISR-MODIS absolute radiometric-scale differences [e.g., *Lyapustin et al.*, 2007]. The MISR team is also exploring ways to improve cloud screening to refine the algorithm's aerosol component and mixture options, to harness more of the multiangle information in retrieving particle properties with the standard algorithm, to retrieve the spectral water-leaving reflectance self-consistently as part of the overwater aerosol retrieval, and to quantitatively assess the performance of the refined algorithm. The MODIS Team is engaged in similar activities, and a larger, community effort is underway to create a long-term, climate quality aerosol data set using the best capabilities of the satellite and suborbital data sets from many sources [e.g., *Diner et al.*, 2004a; Z. Li and T. Zhao, GEWEX Aerosol Working Group organization meeting, September, 2006].

[92] **Acknowledgments.** We thank our colleagues on the Jet Propulsion Laboratory's MISR instrument team and at the NASA Langley Research Center's Atmospheric Sciences Data Center for their roles in producing the MISR data sets. We also thank Brent Holben and Jeff Reid for valuable comments on the manuscript, Lorraine Remer of the MODIS Team for insights regarding the MODIS aerosol retrieval algorithm, Sasha Smirnov for his quality assessment of the AERONET data used in this study, the AERONET Ascension Island, Forth Crete, and Tahiti site managers for providing their valuable data, and the NOAA Air Resources Laboratory (ARL) for providing HYSPLIT model results via the READY website (http://www.arl.noaa.gov/ready.html). This research is supported in part by NASA's Climate and Radiation Research and Analysis Program, under H. Maring, NASA's Atmospheric Composition Program, under P. DeCola, and the EOS-MISR instrument project. It is performed at the Jet Propulsion Laboratory, California Institute of Technology, under contract with NASA.

References

Abdou, W. A., D. J. Diner, J. V. Martonchik, C. J. Bruegge, R. A. Kahn, B. J. Gaitley, K. A. Crean, L. A. Remer, and B. Holben (2005), Comparison of coincident Multiangle Imaging Spectroradiometer and Moderate Resolution Imaging Spectroradiometer aerosol optical depths over land and ocean scenes containing Aerosol Robotic Network sites, *J. Geophys. Res.*, *110*, D10S07, doi:10.1029/2004JD004693.

Anderson, T. L., R. L. Charlson, D. M. Winker, J. A. Ogren, and K. Holmen (2003), Mesoscale variations of tropospheric aerosols, *J. Atmos. Sci.*, *60*, 119–136.

Barnes, W. L., T. S. Pagano, and V. V. Salomonson (1998), Prelaunch characteristics of the Moderate Resolution Imaging Spectroradiometer (MODIS) on EOS-AM1, *IEEE Trans. Geosci. Remote Sens.*, *36*, 1088–1100.

Bogumil, K., et al. (2003), Measurements of molecular absorption spectra with the SCHIAMACHY pre-flight model: Instrument characterization and reference data for atmospheric remote-sensing in the 230–2380 nm region, *J. Photochem. Photobiol. A: Chem.*, *157*, 167–184.

Bréon, F. M., and N. Henriot (2006), Spaceborne observations of ocean glint reflectance and modeling of wave slope distributions, *J. Geophys. Res.*, *111*, C06005, doi:10.1029/2005JC003343.

Bruegge, C. J., W. A. Abdou, D. J. Diner, B. J. Gaitley, M. C. Helmlinger, R. A. Kahn, and J. V. Martonchik (2003), Validating the MISR radiometric scale for the ocean aerosol science communities, in *Proceedings of the International Workshop on Radiometric and Geometric Calibration, December 2–5, 2003, Gulfport, Mississippi*, pp. 103–115, A. A. Balkema, Brookfield, Vt.

Christopher, S., and J. Wang (2004), Intercomparison between multi-angle imaging spectroradiometer (MISR) and Sunphotometer aerosol optical thickness in dust source regions over China: Implications for satellite aerosol retrievals and radiative forcing calculations, *Tellus, Ser. B*, *56*, 451–456.

Chu, D. A., Y. J. Kaufman, C. Ichoku, L. A. Remer, D. Tanré, and B. N. Holben (2002), Validation of MODIS aerosol optical depth retrieval over land, *Geophys. Res. Lett.*, *29*(12), 8007, doi:10.1029/2001GL013205.

Cox, C., and W. Munk (1954), Statistics of the sea surface derived from Sun glitter, *J. Mar. Res.*, *13*, 198–227.

Diner, D. J., et al. (1998), Multi-angle Imaging Spectroradiometer (MISR) instrument description and experiment overview, *IEEE Trans. Geosci. Remote Sens.*, *36*, 1072–1087.

Diner, D. J., et al. (1999a), *MISR Level 2 Aerosol Retrieval Algorithm Theoretical Basis*, *JPL D11400*, Rev. D, Jet Propul. Lab., Calif. Inst. of Technol., Pasadena, Calif. (Available at http://eospso.gsfc.nasa.gov/eos_homepage/for_scientists/atbd/)

Diner, D. J., W. Abdou, H. Gordon, R. Kahn, Y. Knyazikhin, J. Martonchik, D. McDonald, S. McMuldroch, R. Myneni, and R. West (1999b), *MISR Level 2 Ancillary Products and Datasets Algorithm Theoretical Basis*, *JPL D13402*, Rev. B, Jet Propul. Lab., Calif. Inst. of Technol., Pasadena, Calif. (Available at http://eospso.gsfc.nasa.gov/eos_homepage/for_scientists/atbd/)

Diner, D. J., W. A. Abdou, J. E. Conel, K. A. Crean, B. J. Gaitley, M. Helmlinger, R. A. Kahn, J. V. Martonchik, and S. H. Pilorz (2001), MISR aerosol retrievals over southern Africa during the SAFARI-2000 dry season campaign, *Geophys. Res. Lett.*, *28*, 3127–3130.

Diner, D. J., et al. (2004a), PARAGON: An integrated approach for characterizing aerosol climate impacts and environmental interactions, *Bull. Am. Meteorol. Soc.*, *85*, 1491–1501.

Diner, D. J., R. A. Kahn, C. J. Bruegge, J. V. Martonchik, W. A. Abdou, B. J. Gaitley, M. C. Helmlinger, O. V. Kalashnikova, and W.-H. Li (2004b), Refinements to MISR's radiometric calibration and implications for establishing a climate-quality aerosol observing system, in *Passive Optical Remote Sensing of the Atmosphere and Clouds IV*, edited by S. C. Tsay, T. Yokota, and M.-H. Ahn, *Proc. SPIE*, *5652*, 57–65.

Dubovik, O., and M. D. King (2000), A flexible inversion algorithm for retrieval of aerosol optical properties from Sun and sky radiance measurements, *J. Geophys. Res.*, *105*, 20,673–20,696.

Dubovik, O., A. Smirnov, B. N. Holben, M. D. King, Y. J. Kaufman, T. F. Eck, and I. Slutsker (2000), Accuracy assessments of aerosol optical properties retrieved from aerosol Robotic Network (AERONET) Sun and sky radiance measurements, *J. Geophys. Res.*, *105*, 9791–9806.

Dubovik, O., B. Holben, T. F. Eck, A. Smirnov, Y. J. Kaurman, M. D. King, D. Tanré, and I. Slutsker (2002), Variability of absorption and optical properties of key aerosol types observed in worldwide locations, *J. Atmos. Sci.*, *59*, 590–608.

Evans, K. F., and G. L. Stephens (1991), A new polarized atmospheric radiative transfer model, *J. Quant. Spectrosc. Radiat. Transfer*, *46*, 413–423.

Fox, D., E. Gonzalez, R. Kahn, and J. Martonchik (2007), Near-surface wind speed retrieval from space-based, multi-angle imaging of ocean Sun glint patterns, *Remote Sens. Environ.*, *107*, 223–231, doi:10.1016/j.rse.2006.10.021.

Gordon, H. R., J. W. Brown, and R. H. Evans (1988), Exact Rayleigh scattering calculations for use with Nimbus-7 Coastal Zone Color Scanner, *Appl. Opt.*, *27*, 862–871.

Grant, I. P., and G. E. Hunt (1968), Solution of radiative transfer problems using the invariant S_n method, *Mon. Not. R. Astron. Soc.*, *141*, 27–41.

Hansen, J. E., and L. D. Travis (1974), Light scattering in planetary atmospheres, *Space Sci. Rev.*, *16*, 527–610.

Holben, B. N., et al. (1998), AERONET: A federated instrument network and data archive for aerosol characterization, *Remote Sens. Environ.*, *66*, 1–16.

Horváth, Á. (2004), Differences between satellite measurements and theoretical estimates of global cloud liquid water amounts, Ph.D. thesis, 215 pp., Dep. of Atmos. Sci., Univ. of Arizona, Tucson, Ariz.

Ignatov, A., P. Minnis, N. Loeb, B. Wielicki, W. Miller, S. Sun-Mack, D. Tanré, L. Remer, I. Laszlo, and E. Geier (2005), Two MODIS aerosol products over ocean on the Terra and Aqua CERES SSF datasets, *J. Atmos. Sci.*, *62*, 1008–1031.

Jovanovic, V. M., M. A. Bull, M. M. Smyth, and J. Zong (2002), MISR in-flight camera geometric model calibration and georectification performance, *IEEE Trans. Geosci. Remote Sens.*, *40*, 1512–1519.

Kahn, R., P. Banerjee, D. McDonald, and D. Diner (1998), Sensitivity of multi-angle imaging to aerosol optical depth, and to pure-particle size

distribution and composition over ocean, *J. Geophys. Res.*, *103*, 32,195–32,213.

Kahn, R., P. Banerjee, and D. McDonald (2001a), Sensitivity of multiangle imaging to natural mixtures of aerosols over ocean, *J. Geophys. Res.*, *106*, 18,219–18,238.

Kahn, R., P. Banerjee, D. McDonald, and J. Martonchik (2001b), Aerosol properties derived from aircraft multiangle imaging over Monterey Bay, *J. Geophys. Res.*, *106*, 11,977–11,995.

Kahn, R. A., B. J. Gaitley, J. V. Martonchik, D. J. Diner, K. A. Crean, and B. Holben (2005a), Multiangle Imaging Spectroradiometer (MISR) global aerosol optical depth validation based on 2 years of coincident Aerosol Robotic Network (AERONET) observations, *J. Geophys. Res.*, *110*, D10S04, doi:10.1029/2004JD004706.

Kahn, R., et al. (2005b), MISR calibration and implications for low-light-level aerosol retrieval over dark water, *J. Atmos. Sci.*, *62*, 1032–1052.

Kalashnikova, O. V., and R. Kahn (2006), Ability of multiangle remote sensing observations to identify and distinguish mineral dust types: 2. Sensitivity over dark water, *J. Geophys. Res.*, *111*, D11207, doi:10.1029/2005JD006756.

Kattawar, G. W., G. N. Plass, and S. J. Hitzfelder (1976), Multiple scattered radiation emerging from Rayleigh and continental haze layers: 1. Radiance, polarization, and neutral points, *Appl. Opt.*, *15*, 632–647.

Kaufman, Y. J., et al. (1997), Passive remote sensing of tropospheric aerosol and atmospheric correction for the aerosol effect, *J. Geophys. Res.*, *102*, 16,815–16,830.

Koepke, P. (1984), Effective reflectance of oceanic whitecaps, *Appl. Opt.*, *23*, 1816–1824.

Levy, R. C., L. A. Remer, D. Tanré, Y. J. Kaufman, C. Ichoku, B. N. Holben, J. M. Livingston, P. B. Russell, and H. Maring (2003), Evaluation of the Moderate-Resolution Imaging Spectroradiomenter (MODIS) retrievals of dust aerosol over the ocean during PRIDE, *J. Geophys. Res.*, *108*(D19), 8594, doi:10.1029/2002JD002460.

Levy, R. C., L. A. Remer, J. V. Martins, Y. J. Kaufman, A. Plana-Fattori, J. Redemann, and B. Wenney (2005), Evaluation of the MODIS aerosol retrievals over ocean and land during CLAMS, *J. Atmos. Sci.*, *62*, 974–992.

Liu, Y., J. A. Sarnat, B. A. Coull, P. Koutrakis, and D. J. Jacob (2004), Validation of Multiangle Imaging Spectroradiometer (MISR) aerosol optical thickness measurements using Aerosol Robotic Network (AERONET) observations over the contiguous United States, *J. Geophys. Res.*, *109*, D06205, doi:10.1029/2003JD003981.

Lyapustin, A., Y. Wang, R. Kahn, R. Wolfe, J. Xiong, K. Thome, A. Smirnov, C. Bruegge, A. Ignatov, and O. Dubovik (2007), Analysis of MODIS-MISR calibration difference: Implications for data fusion, *Remote Sens. Environ.*, *107*, 12–21, doi:10.1016/j.rse.2006.09.028.

Martonchik, J. V., D. J. Diner, R. Kahn, M. M. Verstraete, B. Pinty, H. R. Gordon, and T. P. Ackerman (1998), Techniques for the retrieval of aerosol properties over land ocean using multiangle data, *IEEE Trans. Geosci. Remote. Sens.*, *36*, 1212–1227.

Martonchik, J. V., D. J. Diner, K. A. Crean, and M. A. Bull (2002), Regional aerosol retrieval results from MISR, *IEEE Trans. Geosci. Remote Sens.*, *40*, 1520–1531.

Martonchik, J. V., D. J. Diner, R. Kahn, B. Gaitley, and B. N. Holben (2004), Comparison of MISR and AERONET aerosol optical depths over desert sites, *Geophys. Res. Lett.*, *31*, L16102, doi:10.1029/2004GL019807.

Mishchenko, M. I., I. V. Geogdzhayev, B. Cairns, B. E. Carlson, J. Chowdhary, A. A. Lacis, L. Liu, W. B. Rossow, and L. D. Travis (2007), Past, present, and future of global aerosol climatologies derived from satellite observations: A perspective, *J. Quant. Spectrosc. Radiat. Transfer*, *106*(1–3), 325–347, doi:10.1016/j.jqsrt.2007.01.007.

Morel, A., and S. Maritorena (2001), Bio-optical properties of oceanic waters: A reappraisal, *J. Geophys. Res.*, *106*, 7163–7180.

Myhre, G., et al. (2005), Intercomparison of satellite retrieved aerosol optical depth over ocean during the period September 1997 to December 2000, *Atmos. Chem. Phys.*, *5*, 1697–1719.

Redemann, J., B. Schmid, J. A. Eilers, R. Kahn, R. C. Levy, P. B. Russell, J. M. Livingston, P. V. Hobbs, W. L. Smith Jr., and B. N. Holben (2005), Suborbital measurements of spectral aerosol optical depth and its variability at subsatellite grid scales in support of CLAMS 2001, *J. Atmos. Sci.*, *62*, 993–1007.

Remer, L. A., et al. (2005), The MODIS aerosol algorithm, products, and validation, *J. Atmos. Sci.*, *62*, 947–973.

Russell, P. B., et al. (1993), Pinatubo and pre-Pinatubo optical depth spectra: Mauna Loa measurements, comparisons, inferred particle size distributions, radiative effects, and relationship to lidar data, *J. Geophys. Res.*, *98*, 22,969–22,985.

Salomonson, V. V., W. L. Barnes, P. W. Maymon, H. E. Montgomery, and H. Ostrow (1989), MODIS: Advanced facility instrument for studies of the Earth as a system, *IEEE Trans. Geosci. Remote Sens.*, *27*, 145–153.

Schmid, B., et al. (2003), Coordinated airborne, spaceborne, and ground-based measurements of massive thick aerosol layers during the dry season in southern Africa, *J. Geophys. Res.*, *108*(D13), 8496, doi:10.1029/2002JD002297.

Seemann, S. W., J. Li, W. P. Menzel, and L. E. Gumley (2003), Operational retrieval of atmospheric temperature, moisture, and ozone from MODIS infrared radiances, *J. Appl. Meteorol.*, *42*, 1072–1091.

Smirnov, A., B. N. Holben, T. F. Eck, O. Dubovik, and I. Slutsker (2000), Cloud-screening and quality control algorithms for the AERONET database, *Remote Sens. Environ.*, *73*, 337–349.

Smirnov, A., B. N. Holben, Y. J. Kaufman, O. Dubovik, T. F. Eck, I. Slutsker, C. Pietras, and R. Halthore (2002), Optical properties of atmospheric aerosol in maritime environments, *J. Atmos. Sci.*, *59*, 501–523.

Wehrli, C. (1985), *Extraterrestrial Solar Spectrum*, *Publ. 615*, World Radiat. Cent. (WRC), Davos-Dorf, Switzerland.

Wolfe, R. E., M. Nishihama, A. J. Fleig, J. A. Kuyper, D. P. Roy, J. C. Storey, and F. S. Patt (2002), Achieving sub-pixel geolocation accuracy in support of MODIS land science, *Remote Sens. Environ.*, *83*, 31–49.

Xiong, X., N. Che, and W. L. Barnes (2006), Terra MODIS on-orbit spectral characterization and performance, *IEEE Trans. Geosci. Remote Sens.*, *44*, 2198–2206.

Yu, H., et al. (2006), A review of measurement-based assessment of aerosol direct radiative effect and forcing, *Atmos. Chem. Phys.*, *6*, 613–666.

Zhang, J., and J. S. Reid (2006), MODIS aerosol product analysis for data assimilation: Assessment of over-ocean Level 2 aerosol optical thickness retrievals, *J. Geophys. Res.*, *111*, D22207, doi:10.1029/2005JD006898.

M. A. Bull, B. J. Gaitley, M. J. Garay, R. A. Kahn, J. V. Martonchik, D. L. Nelson, and K. K. Yau, Jet Propulsion Laboratory, California Institute of Technology, 4800 Oak Grove Drive, Pasadena, CA 91109, USA. (ralph.kahn@jpl.nasa.gov)

R. C. Levy, NASA Goddard Space Flight Center, Greenbelt, MD 20771, USA.